Russian Journal of Earth Sciences

# On Seismic Monitoring Of Dynamic Overpressure Zones In Shallow Marine Sediments

**S. A. Tikhotskiy[1,2], I. O. Bayuk[*,1,2], N. V. Dubinya[*,1,2], S. V. Fomichev[1,2], D. Y. Kuprin[2], and I. A. Voronov[2]**

[1]Moscow Institute of Physics and Technology, National Research University, Dolgoprudny, Russia
[2]Schmidt Institute of Physics of the Earth of the Russian Academy of Sciences, Moscow, Russia
* **Correspondence to:** Irina Bayuk, ibayuk@yandex.ru; Nikita Dubinya, Dubinya.NV@gmail.com.

**Abstract:** The paper presents an algorithm for reconstruction of stress state parameters of rock massif based on data on natural fractures. For one well developing an oil field, the directions of the principal in-situ stresses, their relative magnitudes, and the strength of the rocks in the near-wellbore space were reconstructed. Stress inversion results are in agreement with other methods of stress estimation, in particular, with the results of the mini-hydraulic fracture test. The inverse problem of stress state estimation is solved using the Monte Carlo method. An algorithm of applying the apparatus of mathematical statistics – the method of moments for determining distribution parameters from the Pearson distribution family – to quantify the ambiguity of the estimation of the directions of the principal stresses and their relative magnitudes is presented. The proposed algorithm can be used for independent reconstruction of stresses for carbonate rocks, provided that there is information about the conductivity of fractures in the rocks of the near-wellbore space to further improve the quality of one-dimensional and three-dimensional geomechanical modeling.

**Keywords:** shallow sediments, offshore fields, anomalous pore pressure, unconsolidated sediments, rock physics modeling.

**Citation:** Tikhotskiy, S. A., I. O. Bayuk, N. V. Dubinya, S. V. Fomichev, D. Y. Kuprin, and I. A. Voronov (2024), On Seismic Monitoring Of Dynamic Overpressure Zones In Shallow Marine Sediments, *Russian Journal of Earth Sciences*, 24, ES5007, EDN: SFZTBR, https://doi.org/10.2205/2024es000958

## Introduction

Zones of anomalous high pore pressure – or overpressure zones for short – are a well-known factor of risks associated with development of hydrocarbon reservoirs. The risks are especially high when dealing with offshore reservoirs, as underbalanced drilling may result into an ecological catastrophe with corresponding consequences *Dugan and Sheahan* [2012], *Zhang et al.* [2018]. While geophysical methods of identifying overpressure zones from geophysical data are well-developed for deep sediments, shallow marine sediments remain a problematic issue due to the difficulties to properly describe all processes taking place in unconsolidated media [*Lee*, 2003]. A number of mechanisms for overpressure zones formation and evolution with time have been proposed, including: disequilibrium compaction, hydrate formation sealing, degasification, buoyancy, hydrothermal pressuring, tectonic movement, overpressure transfer, hydrate decomposition, diagenesis, hydrocarbon generation, microbial gas production, microbial plugging as summed up in [*Li et al.*, 2022a]. Glacial decomposition and loading may serve as another mechanism of overpressure build-up in certain areas [*Wangen*, 2021].

Overpressure transfer – fluid migration due to permeability difference that has been witnessed at New Jersey continental slope [*Dugan and Flemings*, 2000]; Yinggehai basin [*Yin et al.*, 2002]; Baram province, Brunei [*Tingay et al.*, 2009] – is of somewhat particular interest among the mentioned factors, since such processes take place at characteristic times of fluid flow. Depending on the conditions, considerable changes in anomalous pore pressure zones overpressure coefficient or positions and sizes of overpressure zones themselves can take

Research Article

Received: 19 September 2024
Accepted: 25 November 2024
Published: 8 December 2024

place in relatively low times – even in months and years. Upward migration of overpressure zones and associated hydromechanical processes have been studied for various regions [*Fan et al.*, 2021; *Liu et al.*, 2022]. It was shown that proper understanding of filtration properties and overpressure coefficients is essential for prediction of overpressure zones presence and migration. According to [*Tingay et al.*, 2009], overpressures can be vertically transferred if an overpressured compartment comes into hydraulic communication with another less pressured and isolated compartment [*Finkbeiner et al.*, 2001; *Grauls and Baleix*, 1994; *Tingay et al.*, 2007]. A mathematical description of such process can be extremely complicated for unconsolidated sediments, where it is obligatory to use poro-elasto-plastic deformation mechanisms, contrary to well-developed poro-elastic coupling of geomechanical and hydrodynamic processes [*Daigle et al.*, 2017; *Liu et al.*, 2022]. It is also worth mentioning that overpressure zones in unconsolidated seafloor sediments tend to achieve hydrostatic state within geological frames of time during sedimentation [*Daigle et al.*, 2017].

The discussed processes may clearly lead to some problems of offshore hydrocarbon reservoirs exploitation and development, not typical for onshore reservoirs. In fact, unconsolidated seafloor sediments tend to show extremely low elasticity limits and almost negligible friction coefficient, hence small changes in the pore pressure lead to development of plastic flow. As a result, overpressure zones have an ability to evolve rapidly, especially during exploration and development leading to the effect of geophysical data "aging": previously obtained data, starting from seismic surveys results can mismatch actual state of unconsolidated sediments containing overpressure zones. Vertical transfer of these zones, changes in their spatial scales and overpressure coefficient level evolution can take place during the typical time scales of reservoir development. Lack of experimental data with prolonged surveys of shallow marine sediments with overpressure zones prevents from construction of a standard methodology of dealing with these issues, as just a few offshore fields with such conditions were reported in corresponding literature (paper [*Li et al.*, 2022a] provides a comprehensive overview of these case studies). At the same time, certain theoretical modeling [*Li et al.*, 2022b] and field observations [*Nifuku et al.*, 2020] provide a basis for such methodology, yet it still lacks a standardized system of verification. In fact, theoretical modeling provides decent data, that can be verified only if a geophysical system of tracking changes in overpressure zones is proposed.

There exist three approaches for the time-lapse seismic monitoring at sea shelf that are different in the acquisition systems used. First and the most conventional is the time-lapse surveys with the towed seismic streamer. It is fast and cheap as compared with the use of the bottom registration systems but also has important disadvantages: only one-component (pressure) registration is possible (therefore only $P$-wave may be used), the noise level is high and the positioning of the receivers are subject to the significant errors. These shortcomings are especially important for the monitoring of the minor changes associated with the overpressure zones evolution. The second approach is associated with the use of the autonomous bottom seismic seismometers (OBS) for the registration. In this case the 3C or 4C (three velocity or acceleration components and pressure) registration is possible and the noise level is significantly lower as compared with the towed streamer. The major disadvantage is the necessity to re-deploy the OBS at each cycle of the time-lapse survey, which is expensive and leads to differences in OBS coordinates between cycles because of the installation errors. The third approach is to use the permanent bottom seismic streamer (BSS), which is installed once before the start of the time-lapse survey and stay in place at the sea bottom for all monitoring period. The data transfer and power supply are provided by bottom cables from coast, ship or drilling platform. The disadvantages of this approach associated with the high price of such systems and their possible damage from ice (at shallow depth's), ship anchors, etc. But the latter possibility also allows for the passive seismic monitoring of the oil field, including the possibility of hydrofracturing monitoring.

The major goal of the current study is to discover the possibility to monitor the overpressure zones evolution with the time-lapse seismic and to compare the OBS and BSS systems with respect to their ability to recover the expected changes in the wavefields.

## Materials and Methods

The basic model for the current research was discussed in [*Tikhotskiy et al.*, 2023] and [*Dubinya et al.*, 2022]. According to [*Dubinya et al.*, 2022], initial data for construction of models of seafloor sediments were obtained from surveys performed at an area located in the northwestern part of the Black Sea. Several exploratory wells were drilled in the area following the completion of marine seismic exploration surveys, as the area was considered to have potential for hydrocarbon deposits [*Bagriy et al.*, 2019].

A prediction of pore pressure was performed using two different approaches. Firstly, the consolidation analysis was performed using a limited set of laboratory experimental data on seafloor sediments samples subjected to external loading. Preconsolidation stress that can be evaluated based on the nonlinearity of stress vs strain curve of unconsolidated geological medium subjected to external stress [*Dugan and Germaine*, 2008; *Saffer et al.*, 2000]. This parameter can be subsequently used to evaluate the pore pressure in the medium in its current state based on its current porosity [*Schneider et al.*, 2009]. Porosity logs were established for a number of exploratory wells with enough logging data using conventional techniques. The resultant pore pressure evaluation is [*Bagriy et al.*, 2019]:

$$P_{\text{por}}(z) = S_v(z) - 10^{-(e-e_0)/C_c}, \tag{1}$$

where $e$ stands for the void ratio, $e_0$ is the void ratio at a vertical effective stress of unity (1 MPa), $C_c$ is the specific compression index describing deformation along the yield surface, and $S_V$ is the total vertical stress.

The second approach described in [*Dubinya et al.*, 2022] is based on rock physics modeling using soft-sand model of *Mavko et al.* [2020] combined with the Gassmann fluid substitution [*Gassmann*, 1951]. A specific effective medium model was introduced with a number of specific parameters determining the dynamic elastic moduli. These parameters include: the pore pressure, elastic moduli of solid grains, porosity, average number of grain–grain contacts, and critical porosity. These parameters are varied in a way to provide the best match between the calculated and observed spatial distributions of dynamic elastic moduli. An independent evaluation of pore pressure at a certain depth obtained from direct observations of drilling process was used to limit the domain of equivalent solutions of the inverse problem for rock physics modeling. As a result, a stochastic solution of rock physics model parameters was obtained providing an opportunity to reconstruct a spatial variations of pore pressure.

Two described methods of pore pressure reconstruction in unconsolidated seafloor sediments were implemented independently. As discussed in [*Bagriy et al.*, 2019], the complete agreement between these methods is impossible due to the difference in the characteristic spatial scales: the unconsolidation analysis is more suitable for detection of small zones (with size of approximately several meters), while the rock physics modeling is dependent on averaging and may be considered as a tool to evaluate the mean anomaly of pore pressure in the studied interval. The resultant estimations of pore pressure changes with depth are shown in Figure 1: black line represents anomaly index of pore pressure (ratio of estimated pore pressure to hydrostatic pressure) for the estimation from rock physics modeling, while gray line is for consolidation analysis obtained from Equation 1.

Based on consequent rock physics modeling, several general zones of considerable overpressure were suggested in [*Tikhotskiy et al.*, 2023]. Corresponding depth intervals are: 6–9 mbsf (zone 1), 13–29 mbsf (zone 2), and 37–43 mbsf (zone 3). The previous study [*Tikhotskiy et al.*, 2023] was mainly focused on the issue of detectability of the lower overpressure zones in presence of the upper zones, namely, is it possible to use seismometer data to find zone 3 from the raw data in presence of anomalies in waveforms caused by presence of zones 1 and 3. The suggested methodology was a construction of synthetic models of elastic properties after two steps: 1) merging of neighboring overpressure zones; 2) manual creation of models where some of these zones are not present ("shutdown" of particular zones meaning an obligatory specification of hydrostatic pore pressure in these

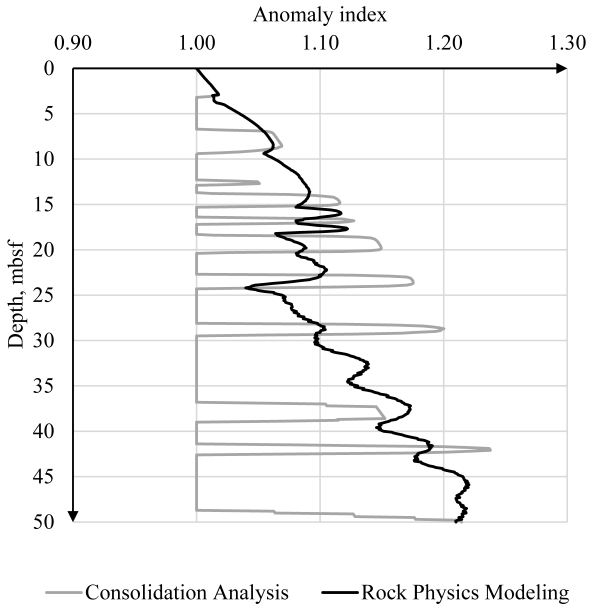


**Figure 1.** Pore pressure anomaly index from two approaches.

zones). Given an established rock physics model – mathematical relationships providing an expected change of elastic moduli of effective medium with changes in pore pressure – synthetic spatial distributions of elastic moduli for these cases can be constructed. It is necessary to mention that only one-dimensional models of properties are studied here given the low number of exploratory wells drilled at site. Therefore, the vertical size of overpressure zone is a crucial factor for subsequent modeling, yet two-dimensional models of overpressure in shallow marine sediments can still be developed in the future to analyze the horizontal scale of anomalous zones.

Generally, the same approach is used in the current study to analyze possible evolution of overpressure zones and opportunities to detect these changes. Since three overpressure zones can be detected on real data, six potentially interesting scenarios of overpressure zones migration upwards and downwards can be suggested for analysis. These scenarios are discussed in Table 1.

**Table 1.** Scenarios for overpressure zones migration

| Scenario | Zone | Pore pressure before migration | Pore pressure after migration |
|---|---|---|---|
| 1. Non-blocked downwards migration at shallow depth. Overpressure zone 1 migrates downwards, to position of zone 2. | 1 | Overpressure | Hydrostatic |
| | 2 | Hydrostatic | Overpressure |
| | 3 | Hydrostatic | Hydrostatic |
| 2. Non-blocked upwards migration at shallow depth. Overpressure zone 2 migrates upwards, to position of zone 1. | 1 | Hydrostatic | Overpressure |
| | 2 | Overpressure | Hydrostatic |
| | 3 | Hydrostatic | Hydrostatic |
| 3. Non-blocked downwards migration at high depth. Overpressure zone 2 migrates downwards, to position of zone 3. | 1 | Hydrostatic | Hydrostatic |
| | 2 | Overpressure | Hydrostatic |
| | 3 | Hydrostatic | Overpressure |
| 4. Non-blocked upwards migration at high depth. Overpressure zone 3 migrates upwards, to position of zone 2. | 1 | Hydrostatic | Hydrostatic |
| | 2 | Hydrostatic | Overpressure |
| | 3 | Overpressure | Hydrostatic |
| 5. Blocked downwards migration at high depth. Overpressure zone 2 migrates downwards, to position of zone 3 with overpressured zone 1. | 1 | Overpressure | Overpressure |
| | 2 | Overpressure | Hydrostatic |
| | 3 | Hydrostatic | Overpressure |
| 6. Blocked upwards migration at high depth. Overpressure zone 3 migrates upwards, to position of zone 2 with overpressured zone 1. | 1 | Overpressure | Overpressure |
| | 2 | Hydrostatic | Overpressure |
| | 3 | Overpressure | Hydrostatic |

There are three general pairs of scenarios. The first pair of scenarios considers the movement of overpressure zone between positions of zones 1 and 2 (downwards migration for scenario 1, and upwards migration for scenario 2). Both cases should have the most notable effect on seismic surveys given the low distance between receiver and anomalous zone. The second pair of scenarios is the same, but the depth is increased (interchanges between positions of zones 2 and 3 are studied here). Independent analysis of this case provides an opportunity to check, whether the depth plays an important role on overpressure zones migration monitoring. Finally, the last pair of scenarios is generally the same as the second pair, but overpressure zone 1 is under consideration. Such analysis provides an opportunity to analyze the "shadowing" effect of overpressure zones previously reported in [*Tikhotskiy et al.*, 2023]: presence of overpressure zones at shallow depths were proven to considerably influence the resultant seismic waveforms receivable by seismometers, which leads to an increased uncertainty in overpressure zones detection. The main idea of the following research lies in comparison of waveforms obtainable before and after the changes in overpressure zone structure and its analysis with regard to typical noise level of seismic data for shallow marine sediments. It is also worth mentioning that the mean level of pore pressure anomaly level in each overpressure zone was taken from Figure 1 without adjustments.

The discussed scenarios are visualized alongside with depth dependencies of the elastic wave velocities, yet it is necessary to provide some information on acquisition of these velocity models obtained from rock physics modeling with manual "shutdown" of certain zones before and after studied dynamic process.

This covers the general workflow used in the current study. It is necessary to generate petroelastic models with reconstructed compressional and shear waves velocities for the discussed scenarios in order to evaluate the overpressure zones migration effect on seismic response of the studied media. Note that for estimation the elastic wave velocities the density provided by log data is used alongside with calculated effective moduli.

The rock-physics model used in [*Dubinya et al.*, 2022] (soft-sand model) was modified in [*Tikhotskiy et al.*, 2023] as follows. Again, a concept of critical porosity was used, which follows from the basic Hertz-Mindlin (HM) model [*Mavko et al.*, 2020]. An unconsolidated rock is considered as a granular medium (dense pack of solid particles) having a critical porosity with so-called "additions". The critical porosity indicates the porosity limit above which a rock becomes unconsolidated. This value was set constant for all depths. The "additions" are inclusions either of suspension or of porous consolidated rock depending on the total porosity. If the total porosity exceeds a critical value at a certain depth, inclusions in the form of a suspension are added to the granular medium. If the total porosity is smaller than the critical value, particles of porous consolidated rock are added in the granular medium. This model differs from a similar model of *Dvorkin et al.* [1999]. Thus, in Dvorkin's model [*Dvorkin et al.*, 1999], in the first case, inclusions of pure fluid (without rock particles) are added to the granular medium instead of suspension inclusions. In the second case, pieces of nonporous mineral material are embedded in the granular medium. As shown in [*Tikhotskiy et al.*, 2023] the modified model is more sensitive to the pore pressure changes compared to the original Dvorkin's model [*Dvorkin et al.*, 1999]. In the model presented in [*Tikhotskiy et al.*, 2023], the porosity values in suspension and consolidated solid material are controlled by so-called "porosity correction coefficient" that is also an unknown model parameter. A sensitivity study of results to this parameter is presented in [*Tikhotskiy et al.*, 2023].

In the model proposed in [*Tikhotskiy et al.*, 2023], for calculating the elastic moduli of a dense pack of rock particles (granular medium), the classical HM model is used. The elastic moduli of suspension are estimated as the lower Hashin-Shtrikman (HS) bound [*Hashin and Shtrikman*, 1963]. For evaluation of the elastic moduli of particles of porous consolidated rock the Berryman's self-consistent method [*Berryman*, 1980] is applied. Having the elastic properties of the granular medium and the "additions", finally, the effective properties of the studied dry rock are obtained. If the suspension inclusions are added (the case when porosity is greater than the critical one) the resulting moduli are calculated as the upper HS bound, since the suspension moduli are lower than the

moduli of dense pack. If the porous pieces of consolidated rock are added in the granular medium (porosity is smaller than the critical), the effective moduli are calculated as the lower HS bound since the porous consolidated rock has lower elastic moduli compared to the granular medium. After the effective elastic moduli of dry rock are calculated as described above, the Gassman's fluid substitution [*Gassmann*, 1951] is applied. Then, the elastic wave velocities $V_p$ and $V_s$ are estimated using the calculated effective elastic moduli and density provided by log data.

For the modeling we use the same model parameters as in [*Tikhotskiy et al.*, 2023]. Namely, the bulk and shear moduli of solid grains are 52 and 32 GPa, respectively. The critical porosity is 60%, coordination number is 18 (average number of contacts of a grain with surrounding grains). The porosity correction coefficient is set to be 1.5. This means that the porosity of suspension is 1.5 times greater than the total porosity and the porosity of consolidated rock is 1.5 times smaller than this value.

Based on consequent rock physics modeling, a distribution of velocities $V_p$ and $V_s$ along the wellbore was obtained for the case of the absence of pore pressure anomalies (Figure 2a) and for cases when the pore pressure anomalies occur in the depth intervals corresponding to zones 1–3 mentioned above (Figure 2b, 2c, 2d). We calculate the pore pressure according to the formula

$$P_{\text{por}}(z) = P_{\text{hydr}} + \text{diff}_p \times A, \tag{2}$$

where $\text{diff}_p$ is the difference between the total vertical stress and hydrostatic pressure and $A$ is a factor ranging from 0 to 1. If $A = 0$, the pore pressure is equal to hydrostatic one (no anomaly in the pore pressure). If $A = 1$, the pore pressure approaches the total vertical stress. Therefore, the greater $A$, the more pronounced is the pore pressure anomaly. For the models shown in Figure 2 we use a fairly high value of the factor $A$, namely, $A = 0.99$. Figure 2 provides a clear view of the overpressure zones effect on elastic waves velocities. High pore pressure considerably decreases the velocities of both $P$- and $S$-waves. The absolute magnitudes of this decrease are roughly the same for both velocities, but, given the low shear wave velocity absolute magnitude for the considered non-consolidated sediments, the relative change in $S$-wave velocity is more considerable compared to $P$-wave velocity.

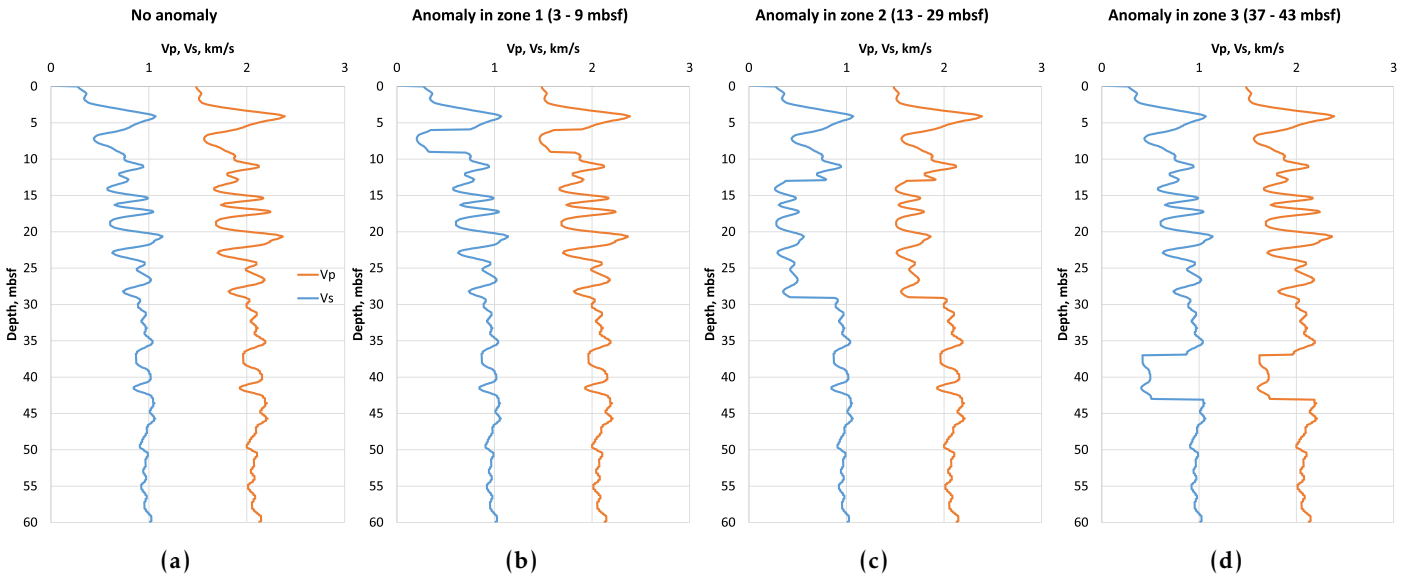


**Figure 2.** Distribution of velocities $V_p$ and $V_s$ along the wellbore. (a) No anomaly in the pore pressure, (b) pore pressure anomaly in zone 1, (c) pore pressure anomaly in zone 2, (d) pore pressure anomaly in zone 3.

The data presented in Figure 2 are subsequently used for seismic modeling to analyze the expected response of the receiver system and its changes associated with transitions of anomalous pressure zones discussed in the previous chapter. For example, the first scenario described in Table 1 can be considered as the transition of velocities distribution shown in Figure 2b to the state depicted in Figure 2c. It is clear that the seismic responses will differ for these two cases, but the magnitude of this difference and its relation with noise cannot be analyzed without direct seismic modeling.

We aim to model the seismic monitoring of the overpressure zones evolution with the bottom seismic registration system that can be represented either by the autonomous bottom seismometers (OBS) or by the bottom seismic streamer (BSS). The both systems may provide the 4C registration, i.e., 3-component velocity (or acceleration) registration and pressure. For the modeling purposes we use the laterally homogeneous 2D elastic media model constructed on the basis of the 1D velocity ($V_p$, $V_s$) and density profiles obtained for the studied scenarios. We suppose the 40-meter water depth and the depth of the seismic source is set to 2 meters below the sea surface. The acquisition system is represented by the 13 bottom 4C receivers separated by 4 meters. The position of the first receiver is below the seismic source thus the maximum source-to-receiver horizontal distance is 48 meters. The described acquisition geometry allows to analyze the behavior of the seismic reflections at different offsets, including the $P$-$S$ converted phases.

The open source SOFI2D software package [*Bohlen*, 2002] is used for the finite-difference modeling of the seismic waves propagation in the above described models. Due to the 2D nature of models only two velocity components ($u_V$, $u_H$) of the sea bottom and water pressure $P$, as recorded by bottom hydrophones, are used for the analysis. The Riecker impulse is used for the modeling with the central frequency of 500 Hz, which is reasonable for the high-resolution marine seismic surveys with the "sparker" source [*Pirogova et al.*, 2019]. With the given central frequency and the lowest velocity of the $S$-waves in model being 200 m/s the smallest wavelength is approximately 0.2 m. The spatial model discretization of 0.02 m (i.e., 10 points per wavelength) is adopted to avoid the numerical dispersion and time step of $5 \times 10^{-6}$ s is used to satisfy the Kramers-Kroening conditions for the simulation stability. The perfect matching layer (PML) conditions are applied to avoid the reverberations.

**Results**

A sensitivity analysis is given here to evaluate the typical changes in elastic waves velocities and other characteristics with alteration of pore pressure. Besides, we also analyze how the pore pressure anomalies can be detected in crossplots of seismic attributes. The reflection coefficients for $P$-wave and converted $P$-to-$S$ wave ($R_{pp}$ and $R_{ps}$, respectively) for the top and bottom of a zone with anomalous pore pressure is analyzed.

An important question is related to the lowest level of pore pressure change that can be registered by seismic receiver data. To analyze how a change in pore pressure can affect the elastic characteristics of unconsolidated rocks we perform a sensitivity study of our rock-physics model to a parameter characterizing a degree of pore pressure anomaly. We vary the pore pressure according to Equation 2. It is worth mentioning that, only within sensitivity analysis, for the purpose of sensitivity study, parameter $A$ is set for the whole model modeling a uniform increase in pore pressure for the whole depth interval, regardless of overpressure zones discussed earlier. We use this approach to numerically evaluate the general sensitivity of the model to changes in pore pressure for the future analysis of the certain overpressure evolution cases.

As it was mentioned and particularly highlighted in Figure 2, overpressure appears to have a strong effect on $P$- and $S$-waves velocities: overpressure zones can be easily seen on anomalies of $V_p$ and $V_s$. Moreover, the ratio of elastic waves velocities $V_p/V_s$ along with the Poisson ratio are also good indicators of overpressure. As it was shown in Figure 2, an increase in the pore pressure results into a simultaneous decrease in compressional and shear waves velocities. As far as the absolute values of velocities drop are comparably same for both $P$- and $S$-waves, and the absolute values of shear waves velocities are much

lower than compressional waves velocities, especially for unconsolidated sediments, it is natural to expect that velocities ratio $V_p/V_s$ and, respectively, the Poisson ratio are good indicator of pore pressure presence which is in line with Figure 2. As seen from Figure 2 the dependencies of the elastic characteristics on the pore pressure change are nonlinear. The characteristics become more sensitive to the anomaly as the anomaly increases. One can say that the $S$-wave velocity exhibits more sensitivity to the pore pressure change. Thus, at depth 40 m, the change in $V_s$ velocity approaches 16% for $A = 0.4$ whereas the respective change in $V_p$ velocity at the depth is around 3%. Since $V_s$ drops more rapidly with the pore pressure anomaly, the $V_p/V_s$ increases. For the largest anomaly in the pore pressure ($A = 0.99$) the $V_p/V_s$ increases almost twice compared to the case when the anomaly is absent (Figure 3c). The Poisson ratio also increases with the pore pressure anomaly and may attain rather high values, namely, 0.45–0.48 (Figure 3b).

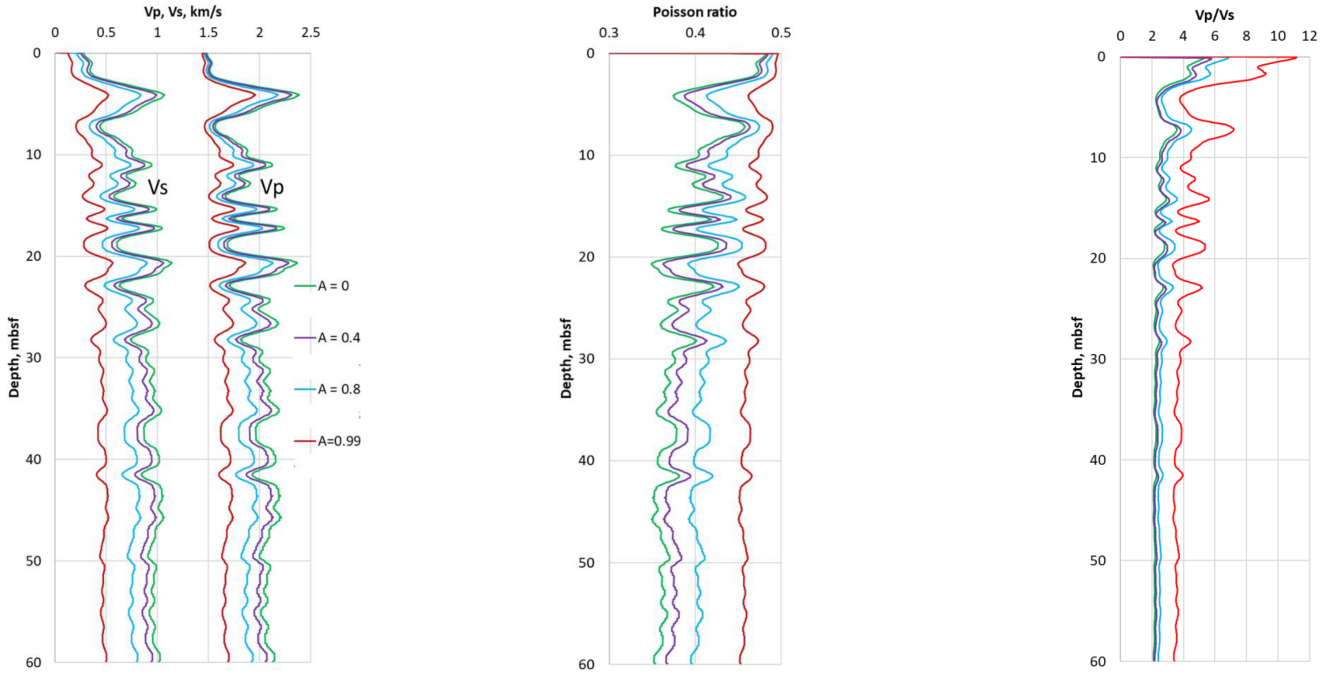


**Figure 3.** Dependencies of elastic properties on factor $A$ characterizing a degree of pore pressure anomaly. (a) Elastic wave velocities $V_p$ and $V_s$, (b) Poisson ratio, (c) $V_p/V_s$.

Figure 4 shows the crossplots of seismic attributes allowing to identify specific shifts of dependencies caused by anomalous pore pressure in the depth interval 13–29 m ($A = 0.99$). The elastic impedance ($A_p$) versus shear impedance ($A_s$), elastic impedance versus $V_p/V_s$, and shear impedance versus $V_p/V_s$ are shown. Orange circles within gray triangles are points corresponding to depths outside the depth interval 13–29 m (without pore pressure anomaly). Orange circles without surrounding triangles correspond to the depth interval with anomalous pore pressure (13–29 meters). Black triangles show the points in the same depth interval (13–29 meters) but for pore pressure without anomaly. Green arrows indicate how the points without pore pressure anomaly shift when the anomaly occurs. As seen this shift is dramatic.

Figure 5 shows the reflection coefficients $R_{pp}$ and $R_{ps}$ for the top and bottom of a zone having anomalous pore pressure at the depths from 37 to 43 m (for $A = 0.99$). Plots (a) and (b) show the $R_{pp}$ and $R_{ps}$ for the top of interval with the enhanced pore pressure, and plots (c) and (d) show $R_{pp}$ and $R_{ps}$ for the bottom of the interval. Red curves are the exact values provided by the Zöeppritz equation (real parts of the coefficients), and blue curves are the Rüger approximation. As seen, the reflection coefficients are rather high and the both boundaries of this anomaly pressure layer can be clearly seen in seismic experiment.

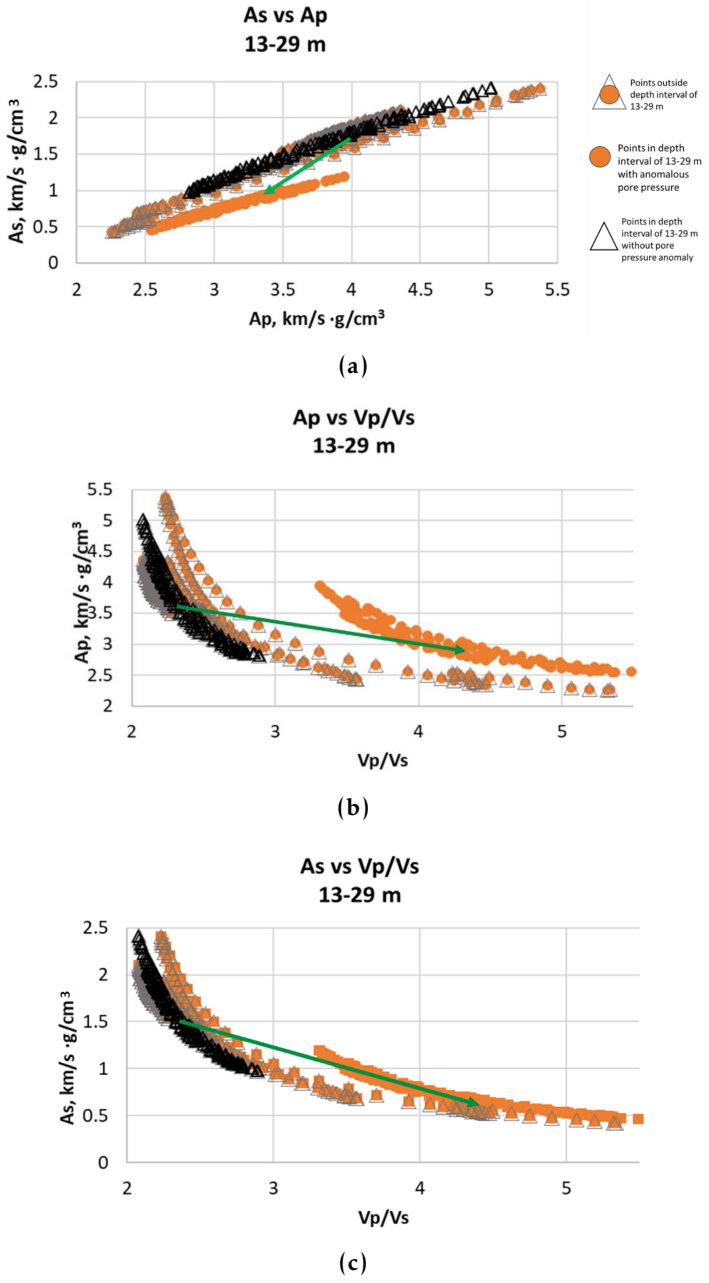


**Figure 4.** Crossplots of seismic attributes for the depth interval 13–29 m. (a) Shear impedance ($A_s$) vs elastic impedance ($A_p$), (b) elastic impedance vs $V_p/V_s$, (c) shear impedance vs $V_p/V_s$. Green arrows indicate how the points without pore pressure anomaly shift when the anomaly occurs.

Here we provide the obtained results and offer some discussion. The modeling results are presented in Figure 6 below. The open-source Seismic Unix software package [*Cohen and Stockwell, Jr.*, 2002] used for the seismograms visualization. The gain correction (multiplication by time) has been applied to all seismograms expect of rot $\overline{u}$ to correct for the geometrical distortion of the wavefields. An example of modeling results is shown in Figure 6 for scenario 1. The figures are organized as follows: each scenario is characterized by 12 figures: four parameters (pressure $P$, 1st row; vertical velocity component $u_V$, 2nd row; horizontal velocity component $u_H$, 3rd row; velocity curl rot $\overline{u}$, 4th row) are provided for initial state of scenario (1st column) and final state of scenario (2nd column); absolute difference is given in the 3rd column for every parameter. Each figure corresponds to its own scenario.

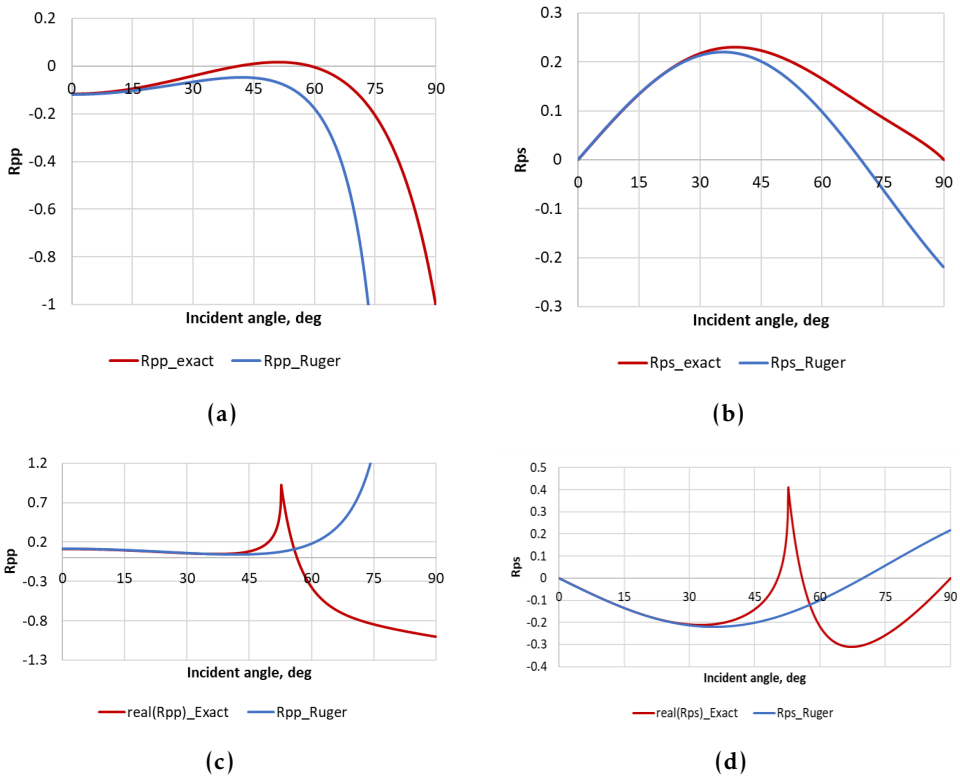


**Figure 5.** Reflection coefficients of the *PP* and *PS* waves ($R_{pp}$ and $R_{ps}$) for the top and bottom of zone having anomalous pore pressure at the depths from 37 to 43 m. (a) $R_{pp}$ and (b) $R_{ps}$ for the top of interval with the enhanced pore pressure; (c) $R_{pp}$ and (d) $R_{ps}$ for the bottom of the interval. Red curves are exact values (the Zöeppritz equations are solved), and blue curves are the Rüger approximation.

As it can be seen (Figure 6) the behavior of the vertical velocity component $u_V$ and pressure $P$ fields are similar. It is reasonable due to the boundary conditions at the sea bottom interface. At small offsets (low reflection angles that do not exceed 35 degrees) these fields are dominated by the $P$-wave energy. As an opposite the horizontal velocity component field $u_H$ at small offsets is dominated by the $S$-wave energy. The increase of the amplitude of the $u_H$ seismograms with offset arise due to two factors: (i) the increase of the $P$-$S$ reflection coefficient with the increase of the reflection angle and (ii) the increase of the horizontal component of the $P$-waves because of the increasing incidence angle of the reflected wave at sea bottom. But the first factor is dominating as it is supported by the similarity of the $u_H$ and rot $\overline{u}$ seismograms. The rot $\overline{u}$ seismograms are the direct indicators of the $S$-wave field as they corresponds to the shape deformation. Therefore, the $u_H$ seismograms recorded by bottom seismometers may be considered as the $S$-wave reflections, including both $S$-$S$ and $P$-$S$ converted phases. As the $S$-wave velocity $V_s$ is approximately twice lower as compared to the $P$-wave velocity $V_p$ in bottom sediments the arrival times of the $S$-wave reflections are higher as compared to that of the $P$-wave reflections, the wavelength of the $S$-wave is also approximately half of that for the $P$-wave and these two factors significantly increase the resolution capabilities of the $u_H$ seismograms as compared to that of $u_V$ and $P$ seismograms as it can be seen in Figure 6a–6i. Moreover, the relative change of the $V_s$ with increasing pore pressure is larger as compared to changes in $V_p$. This factor also contributes to the more prominent demonstration of overpressure zones and their evolution in $u_H$ seismograms. Let us analyze in more detail the scenario 1 (Figure 6). In the starting model the overpressure zone is 3 meters thick with its top at 6 m and bottom at 9 m. At the $u_H$ seismogram (Figure 6g) it is seen from the $S$-$S$ reflection from top (phase starting at 0.05 s at $x = 4$ m) and from bottom (phase starting at 0,065 s at $x = 4$ m). The intermediate reflected phase starting at 0.58 s at $x = 4$ m

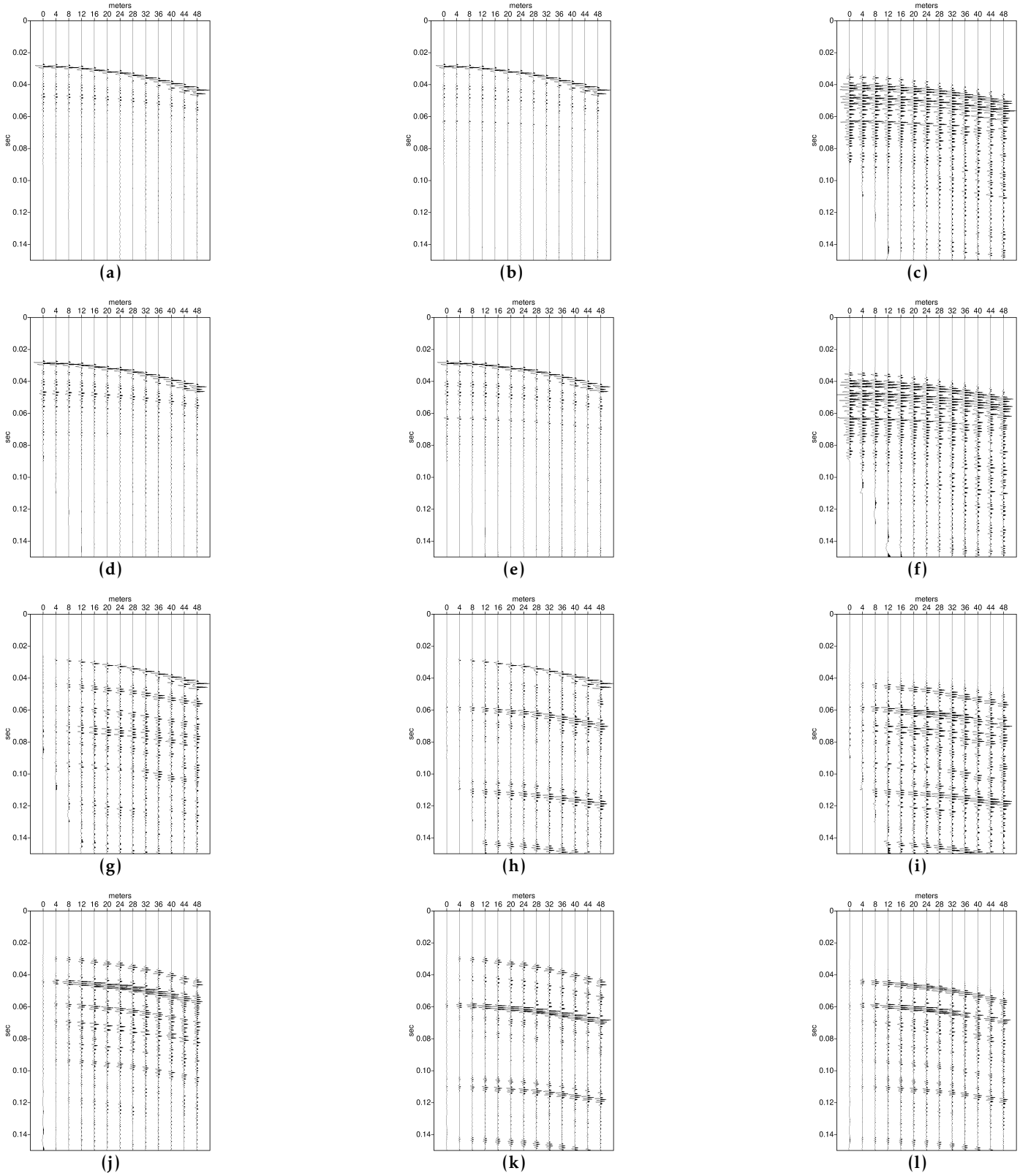


**Figure 6.** Reflection coefficients of the $PP$ and $PS$ waves ($R_{pp}$ and $R_{ps}$) for the top and bottom of zone having anomalous pore pressure at the depths from 37 to 43 m. (a) $R_{pp}$ and (b) $R_{ps}$ for the top of interval with the enhanced pore pressure; (c) $R_{pp}$ and (d) $R_{ps}$ for the bottom of the interval. Red curves are exact values (the Zöeppritz equations are solved), and blue curves are the Rüger approximation.

corresponds to the $P$-$S$ converted phase reflected from zone bottom. Below reflections are less prominent because of the absence of the strong reflectors in the model below the overpressure zone (Figure 6g). In the final model the overpressure zone moves downward, becomes 16 meters thick and has its top at 13 m and bottom at 29 m. The pattern of the $u_H$ (Figure 6h) clearly changes and reflects the new overpressure zone configuration. The zone top is seen from the strong $S$-$S$ reflection phase starting at 0.06 s at $x = 4$ m, the zone bottom is seen from the $P$-$S$ converted reflection phase starting at 0.11 s at $x = 4$ m and $S$-$S$ reflection phase starting at 0.145 s at $x = 8$ m (the difference of the minimum offset that allows to see the phase is due to the decrease of the reflection angle with the increasing reflector depth). All mentioned changes in the $u_H$ reflection pattern leads to the sharp picture at the wavefields difference seismogram (please note the perfect compensation of the direct arrival phase).

At the $P$ and $u_V$ seismograms (Figure 6a–6f) the corresponding changes can be also seen. Specifically, in the seismogram that corresponds to the final model the wave reflected from the overpressure zone bottom at 29 m arises at 0.06 s. But it appears to be difficult to resolve the model structure and its evolution in the upper part of the model. This is partially because of the larger wavelength of the $P$-wave: for the mean velocity of 2000 m/s the central wavelength at 500 Hz is 4 m which is comparable to the thickness of the overpressure zone in the starting model and the difference between the zone bottom (9 m) in the starting model and its top (13 m) in the final model. Therefore, it is difficult to resolve these features and their changes in the $P$-wave field. The difference $P$-wave field (Figure 6f) possesses complex pattern without the clear separated phases due to the interference of the longer waves separated by smaller intervals, as compared to $S$-wave field (Figure 6i).

Analysis of the seismograms associated with other 5 scenarios (Figures A1–A5) leads to the same conclusions. The structure and evolution of the overpressure zones in the shallow submarine sedimentary layers are much more visible in the horizontal velocity component $u_H$ wavefield as compared to the pressure $P$ and vertical velocity $u_V$ seismograms. This emphasizes the preference of the 4C bottom registration systems over conventional 1C (typically hydrophone pressure) registration.

Another important question is the effect of the errors in bottom seismometers positioning on the overall quality of the overpressure zones monitoring. This question is highly important in the context of the comparison between the possibilities of the autonomous bottom seismometers (OBS) and the bottom seismic streamer (BSS) registration systems. With the OBS one needs to deploy them before the seismic survey and then remove the installation in order to read data and charge batteries. In the case of time-lapse seismic monitoring this leads to the necessity for the OBS deployment before each survey cycle. There is no such problem with the BSS system: once deployed it will be in place for all cycles. Currently the typical accuracy of the OBS installation with respect to survey plan is 10% of the water depth. We simulate this situation by shifting the receiver position for the final models (i.e., simulated second cycle of the time-lapse survey) of the overpressure evolution scenarios by random value in the range of ±3 meters (less than 10% of the 40 m water depth) as compared to their position at the initial state. The modeling results are presented in Figure 7 for scenario 1. It is clear that errors in OBS positioning lead to the changes in seismograms that mask the changes associated with the overpressure zones evolution. This is especially visible in the difference seismograms, where the phase correlations are destroyed because of the destructive interference that appears due to the OBS shift. This effect is more drastical in the pressure differential seismograms (Figure 7c). The same effects can be observed for the other studied scenarios.

Results of the seismic modeling leads to some important conclusions. First, the time-lapse seismic is capable to monitor the evolution of the overpressure zones in shallow submarine sediments. Typical "sparker" seismic source with the 500 Hz mean frequency that is widely used in high-resolution marine surveys and provides the possibility to image the upper 100–200 meters under the sea bottom [*Pirogova et al.*, 2019] may be used for

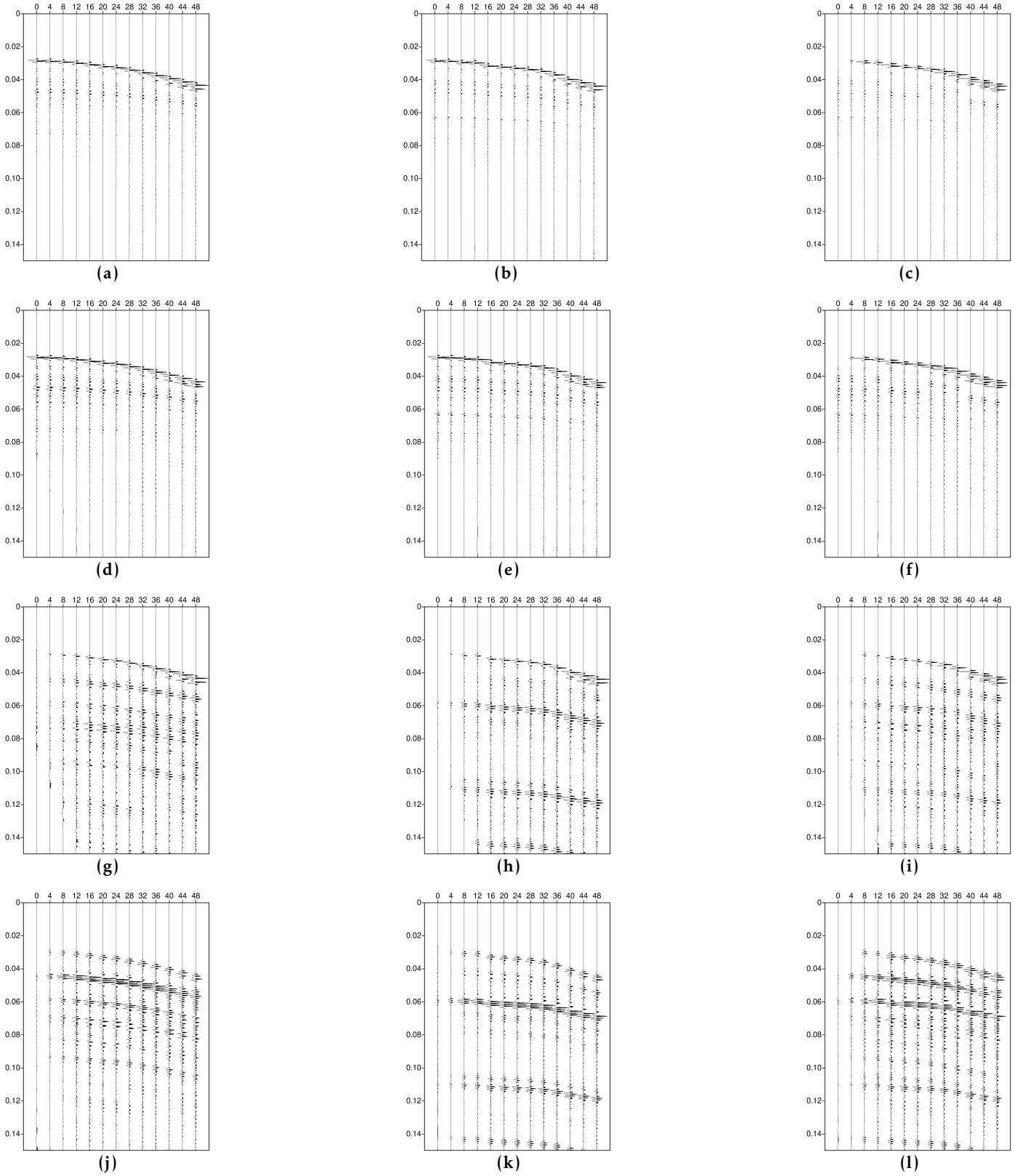


**Figure 7.** Wavefields, adjusted positions: (a) pressure before transition; (b) pressure after transition; (c) pressure difference; (d) vertical velocity before transition; (e) vertical velocity after transition; (f) vertical velocity difference; (g) horizontal velocity before transition; (h) horizontal velocity after transition; (i) horizontal velocity difference; (j) velocity curl before transition; (k) velocity curl after transition; (l) velocity curl difference.

this purpose. Second, the horizontal component of the wavefield is the most informative and provides the best resolution because it is dominated by the *S*-wave with the lower velocity and wavelength. The most conventional hydrophone measured pressure wavefield is less informative especially for the thin overpressure zones and minor changes in their position. Therefore, the 3C or 4C registration at the sea bottom is highly preferable for the overpressure zones study and monitoring. Third, the bottom seismic streamer (BSS) registration system that is once deployed at the sea bottom and used in all cycles of the time-lapse seismic has the clear preference at the autonomous bottom seismometers (OBS) that must be re-installed before each survey cycle. The reason is the unreliable differences between the actual OBS installation coordinates at different cycles that lead to the destruction of the reflection phase in the difference wavefield.

**Discussion**

The obtained results provide an opportunity to analyze the possibilities of geophysical monitoring systems to track migrations of overpressure zones in shallow marine sediments. The plotted seismograms highlight the relative changes in the data that will be received by monitoring systems before and after migration of overpressure zones according to each of studied scenarios. Visual comparison of two sets of seismograms – for adjusted and non-adjusted receiver positions shown in Figures 6 and 7 – is important from the practical point of view. It was shown that a small adjustment of receiver positions alters the registered seismic response comparably with the alterations caused by migration. This effect is especially considerable when there is a static overpressure zone located in the upper part of the studied region: it "overshadows" the migration of overpressure zones in the bottom layers, increasing the demands on the quality of receiver data. As a result, wrong positioning of seismometers for a repeated survey can lead to false conclusions on stationary overpressure zones when they are in fact migrating.

Comparison of Figures 6 and A1 reveals a significant effect of migration direction on observed data. It appears that upwards migration is associated with more significant changes in the wavefield compared to downwards migration The same is true for Figures A2 and A3 yet the effect is not that considerable due to increase in distance between the overpressure zones and receiver positions. Moreover, as it follows from Figures A4 and A5, presence of static overpressure zones above the changing zone decreases the chances to reveal the migration process. The size of the overpressure zone itself plays an important role in detection possibilities, given that it is seemingly easier to detect overpressure zone transition for scenarios 1 and 4 compared to scenarios 2 and 3 (for the first pair the final state contains a large overpressure zone 2, and for the second pair this zone is only present in the initial state). Although it was discussed above that horizontal velocity is the most prominent parameter to deal with overpressure zones evolution detection, some cases allow vertical velocity to provide valuable information as well. As Figures 6, A1, and A3d, A3e, A3f suggest, the cases with the most notable changes in wavefields (scenarios 1, 2, and 3) provide enough information to guess overpressure zone transition direction for the least from vertical velocity. Nevertheless, this factor is way less distinct compared to horizontal velocity.

Seismometer positioning appears to play a crucial role in the problem of monitoring the state of overpressure zones in shallow marine sediments. Difficult conditions at offshore reservoirs are a source of various obstacles preventing repeated seismic surveys to be performed with receivers at exactly same positions as for the initial surveys. Nevertheless, this obstacle can be overcome with an installation of permanent seismic monitoring system. Such system considerably decreases the possible positioning errors providing enhanced possibilities to track subtle changes in overpressure zones migration. In addition to decreased uncertainty in receiver positions, such system may provide even more detailed analysis of hydromechanical processes taking place in shallow marine sediments. Namely, permanent monitoring system can provide way more data than the two cases (before and after migration of overpressure zines) considered in the current study. Early signs of

overpressure zone migration can be detected using such systems. This opportunity becomes even more important for upwards migration of overpressure zones, especially near seafloor, which is one of the most preferable scenarios from the anomaly migration tracking point of view. The discussed case may be important with respect to prevention of ecologically undesirable processes of gas migration to sea water due to the effects associated with offshore hydrocarbon reservoirs exploitation. Installment of permanent seismic monitoring system can reduce ecological risks due to the given opportunity of early detection and prediction of overpressure zones upwards migration. Nevertheless, methodical studies similar to the reported one should be preliminarily performed at certain sites to design the monitoring systems in accordance with specifics of the considered regions, starting from mechanical properties of seafloor sediments, their consolidation level, and severity of overpressure near seafloor.

**Conclusions**

The reported study is devoted to various aspects of seismic monitoring of the overpressure zones evolution in shallow marine sediments. Such sediments are often characterized by low level of sedimentation which implies extra difficulties on the problem of pore pressure prediction from geophysical data – an important problem for safe and efficient exploitation and development of offshore hydrocarbon reservoirs.

Rock physics modeling was proved as a decent tool for utilizing geophysical data for prediction of overpressure zones in seafloor sediments at shallow depths (up to several dozens of meters below seafloor), yet considerable changes are to be introduced to the modeling process, since the studied sediments are unconsolidated, and complicated models should be used contrary to the models frequently used for pore pressure prediction in consolidated rock masses. Rock physics modeling could also answer the question "What if…?". In this particular study this question was clarified: "What if estimated overpressure zones start migrating?". The answer to this question is generally clear: observable geophysical fields – starting from seismic response of the medium – can change if pore pressure is redistributed within seafloor sediments due to natural or external reasons. The changes in compressional and shear waves velocities considered within the sensitivity study analysis prove to be considerable. The ratio $V_p/V_s$ appears to be an extremely sensitive parameter that can be addressed as one of the most reliable seismic indicator of overpressure zones.

The basic model of mechanical properties of seafloor sediments with overpressure zones has been established in the previous studies. This model was used as a basis for introducing several scenarios of overpressure zones evolution, namely their upwards and downwards migration. These changes were analyzed from the perspective of seismic response of the medium. The obtained results support the idea that the multi-component seismic registration at sea bottom is needed to better identify and monitor the evolution of pore pressure zones, because the horizontal component of the wavefield is more informative for this purpose. Bottom seismometers have been already proposed as a tool for detection of overpressure zones in the previous study, but seismometers themselves cannot provide enough information track changes in pore pressure spatial redistribution. It appears that repetitive seismic surveys at the same sites can be performed, but the errors in seismic responses implied by technical uncertainties in receiver positioning are of the same level as changes in seismic surveys caused by overpressure zones evolution. As a result, it is difficult to distinguish apparent changes in seismic response caused by technical procedures, from changes caused by natural reasons.

Introduction of permanent seismic monitoring systems installment to seafloor may be a decent solution of the mentioned problem due to a number of reasons discussed in the discussion section of the paper. Usage of such systems can decrease geological and ecological risks of offshore hydrocarbon reservoirs exploitation and development with corresponding increase in economic efficiency.

**Acknowledgments.** This research was founded by the Russian ministry of science and higher education, contract number 075-11-202-030 from 8 April 2022.

## Appendix A

We would like to put the majority of the seismic modeling results here, as the obtained figures are generally similar. In a same way as for Figure 6 we present seismic modeling results in a form of seismograms for scenarios 2–6 from Table 1 (Figures A1–A5 respectively). The figures are organized similarly to Figure 6 as well: each scenario results contain initial (left column), final (middle column) states and difference (right column) four parameters: pressure (1st row), vertical velocity (2nd row), horizontal velocity (3rd row), and velocity curls (4th row). Figures A6–A10 depict the same parameters for the adjusted positions of the receivers similarly to Figure 7.

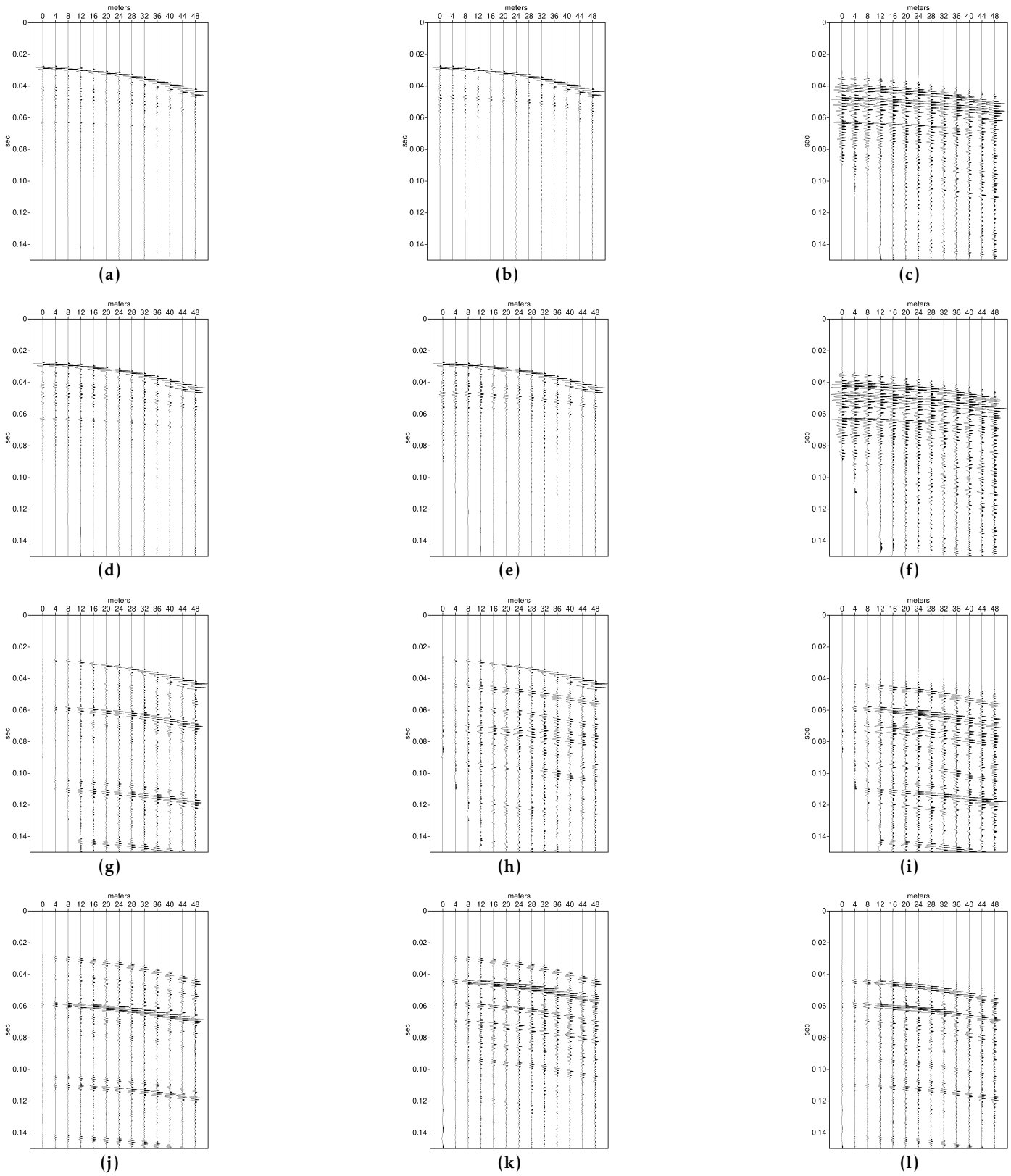


**Figure A1.** Wavefields for scenario 2: (a) pressure before transition; (b) pressure after transition; (c) pressure difference; (d) vertical velocity before transition; (e) vertical velocity after transition; (f) vertical velocity difference; (g) horizontal velocity before transition; (h) horizontal velocity after transition; (i) horizontal velocity difference; (j) velocity curl before transition; (k) velocity curl after transition; (l) velocity curl difference.

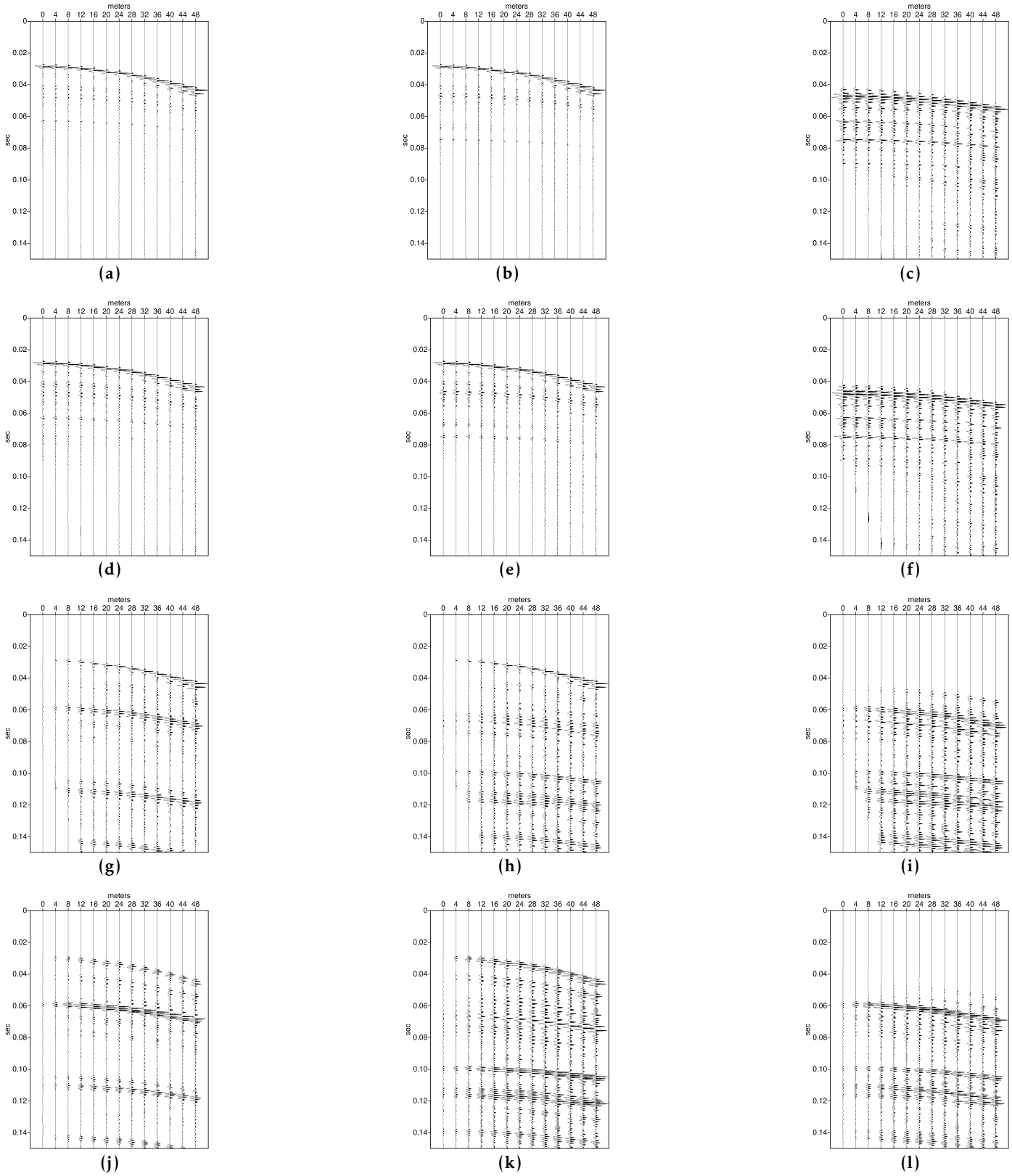


**Figure A2.** Wavefields for scenario 3. Legend is the same as for Figure A1.

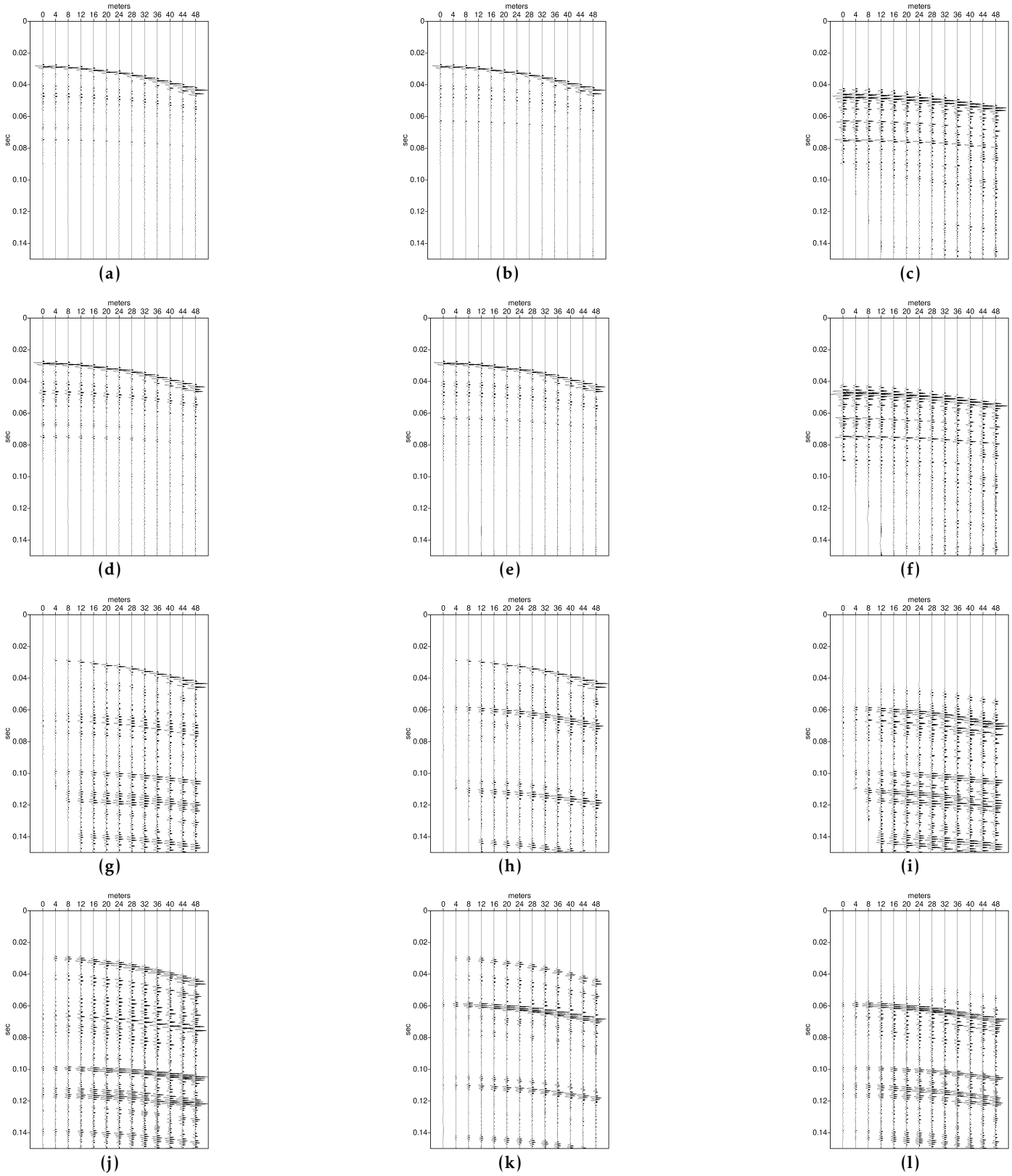


**Figure A3.** Wavefields for scenario 4. Legend is the same as for Figure A1.

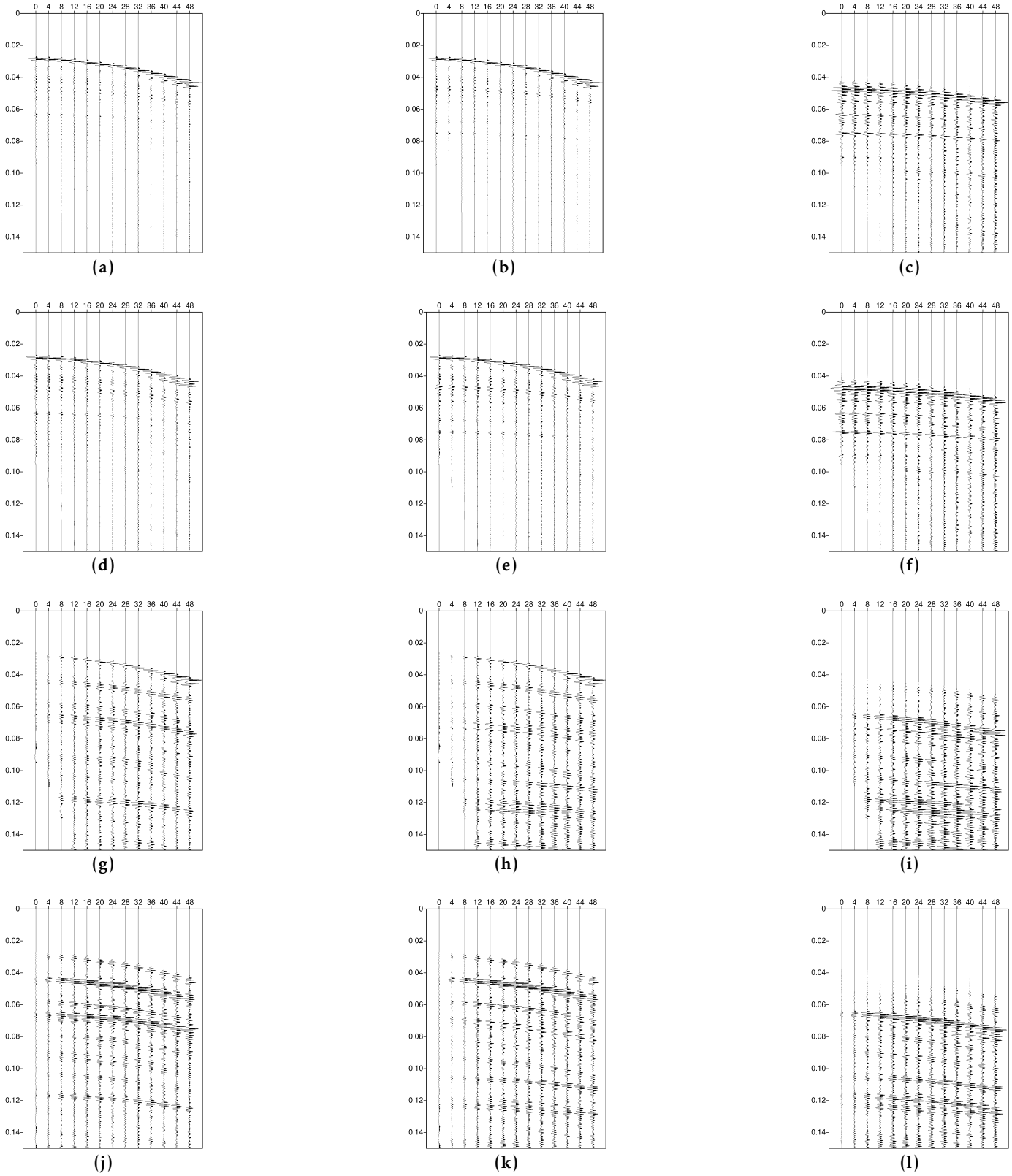


**Figure A4.** Wavefields for scenario 5. Legend is the same as for Figure A1.

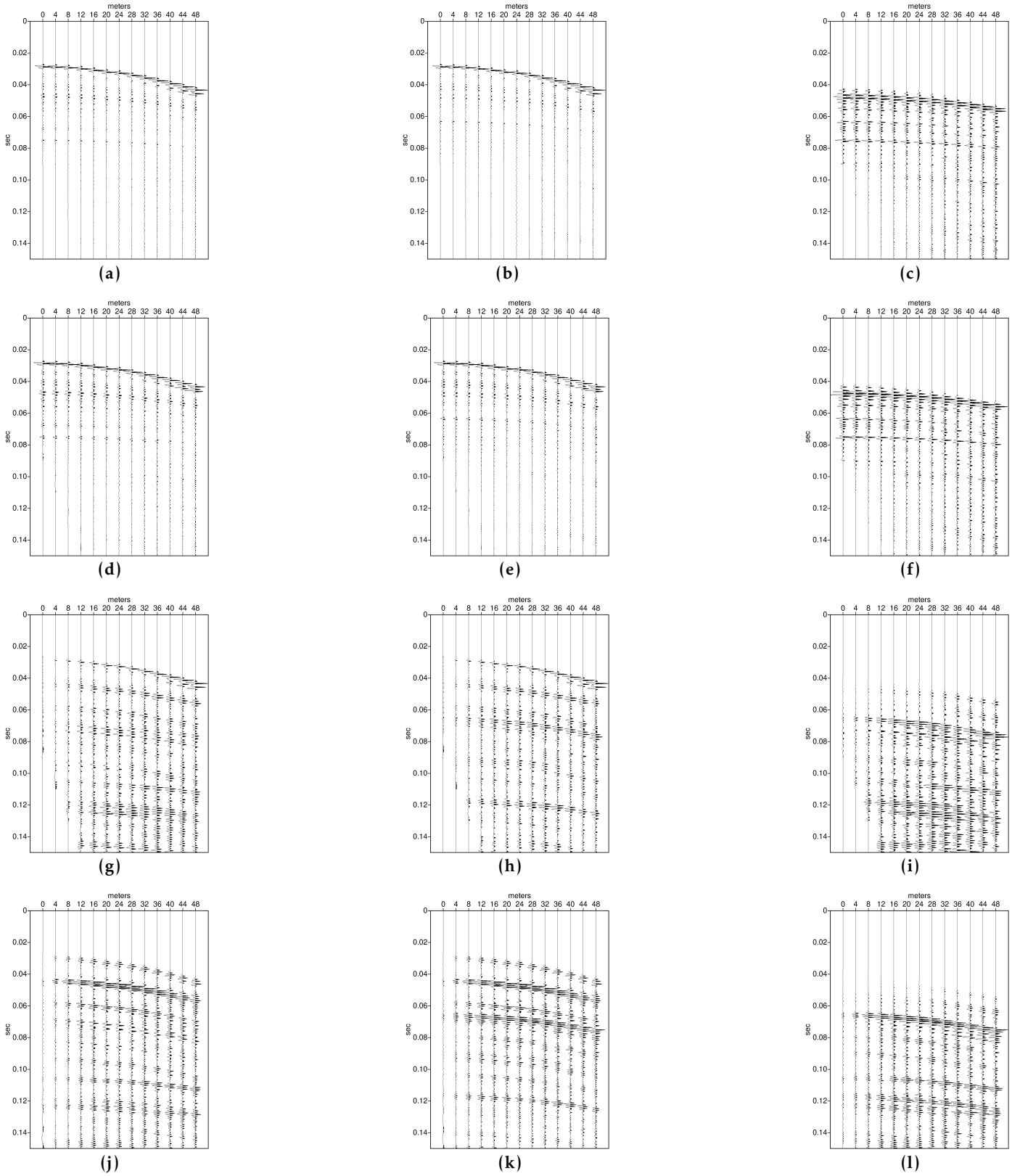


**Figure A5.** Wavefields for scenario 6. Legend is the same as for Figure A1.

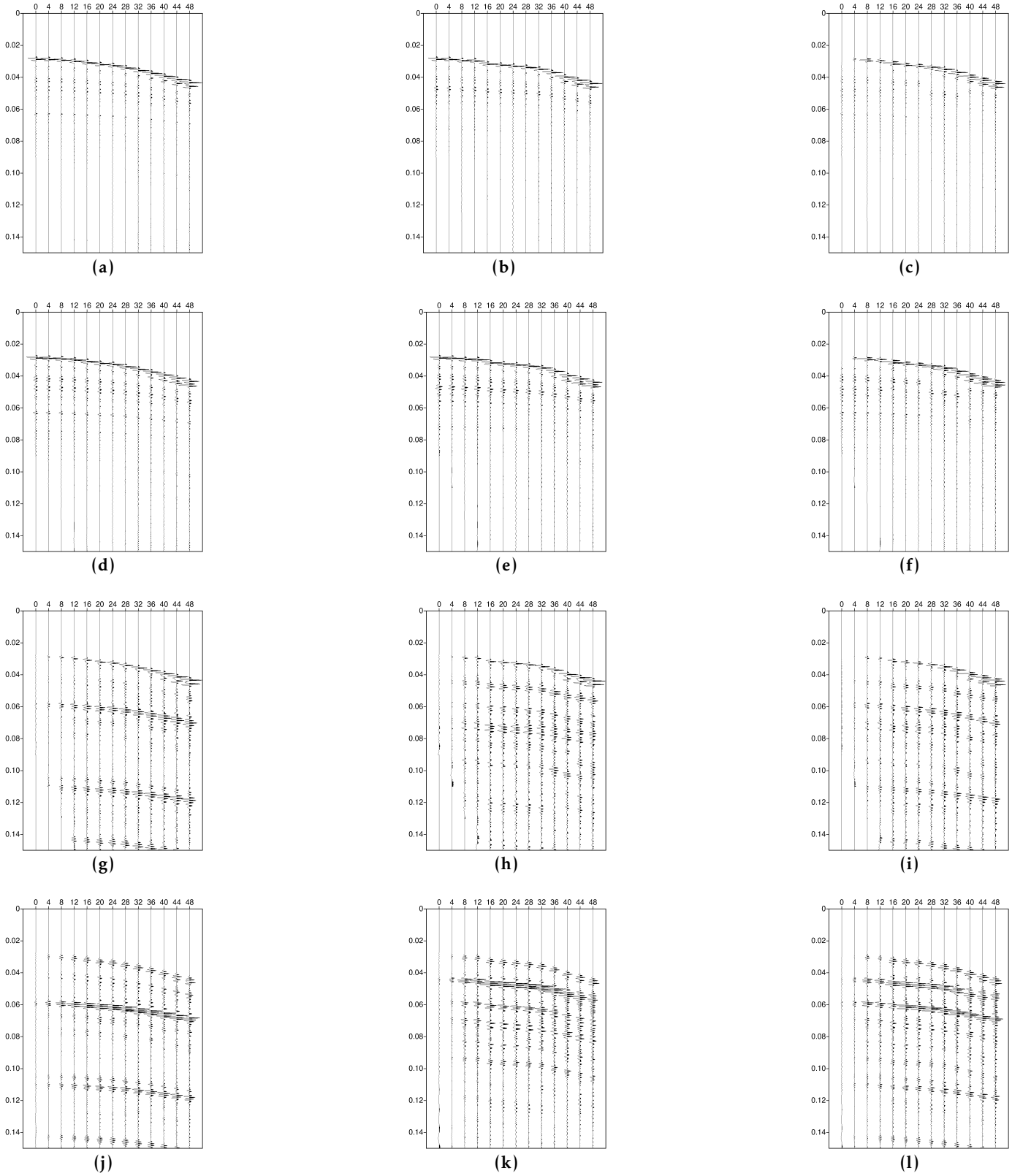


**Figure A6.** Wavefields for scenario 2 with adjusted positions. Legend is the same as for Figure A1.

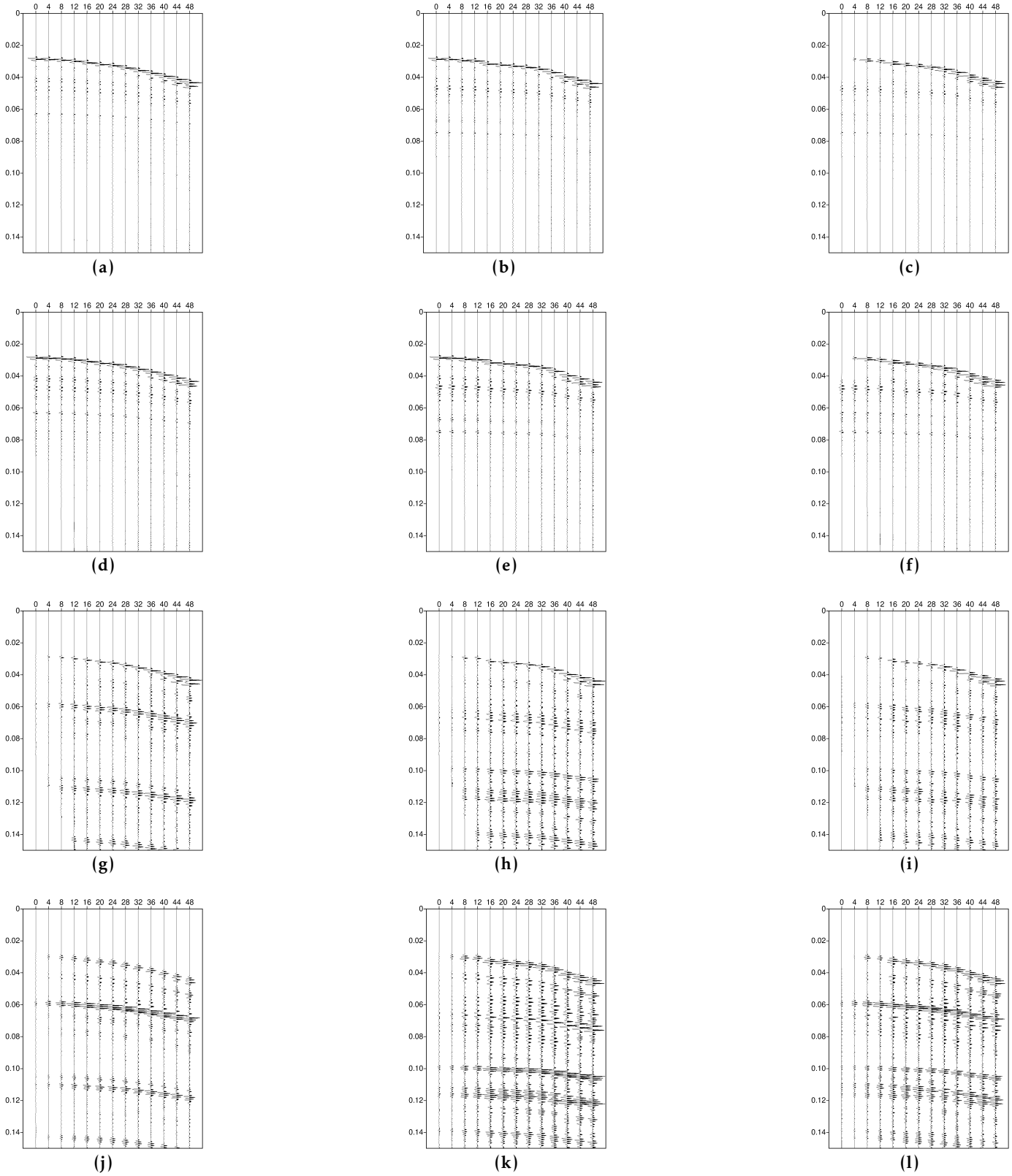


**Figure A7.** Wavefields for scenario 3 with adjusted positions. Legend is the same as for Figure A1.

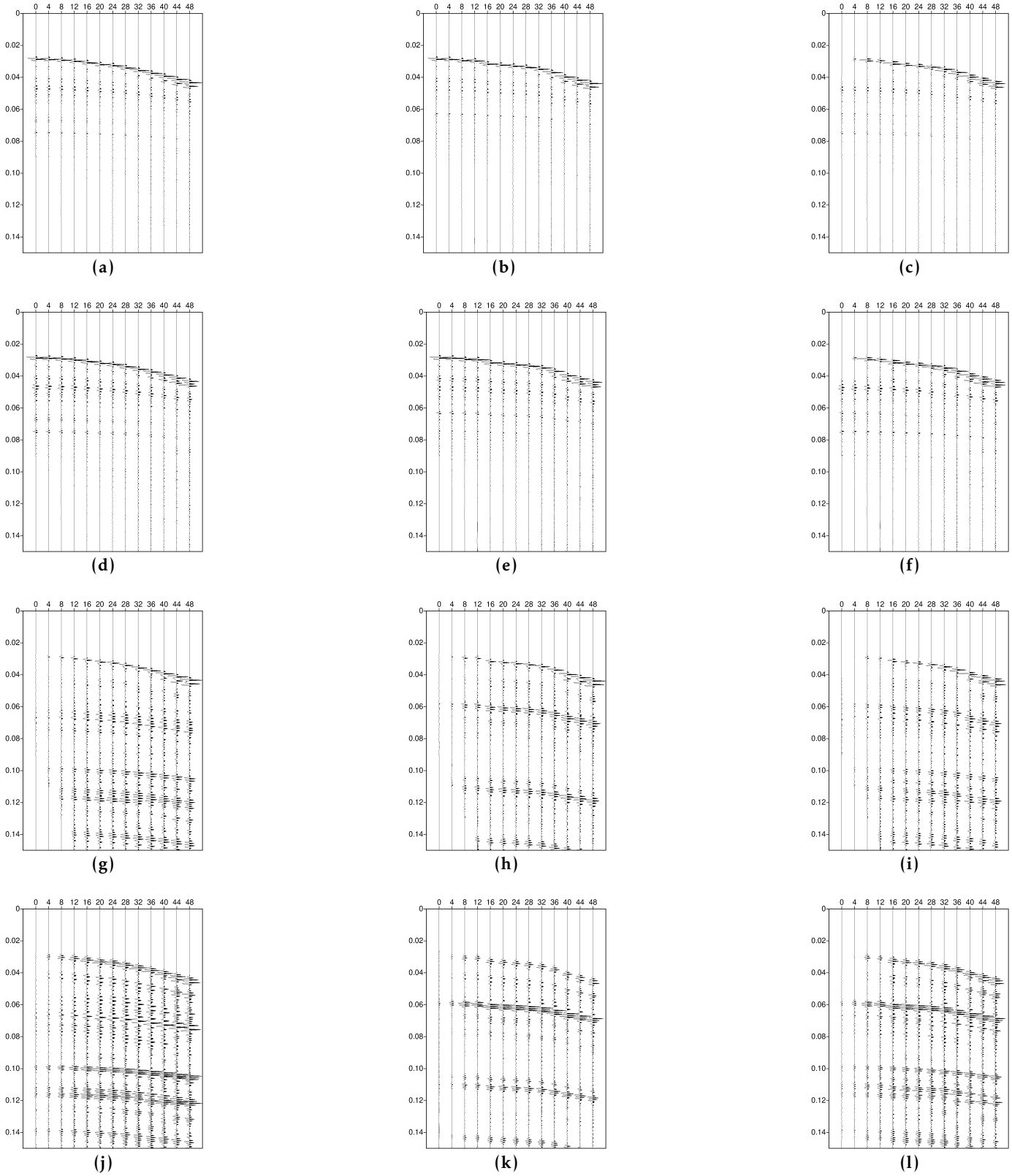


**Figure A8.** Wavefields for scenario 4 with adjusted positions. Legend is the same as for Figure A1.

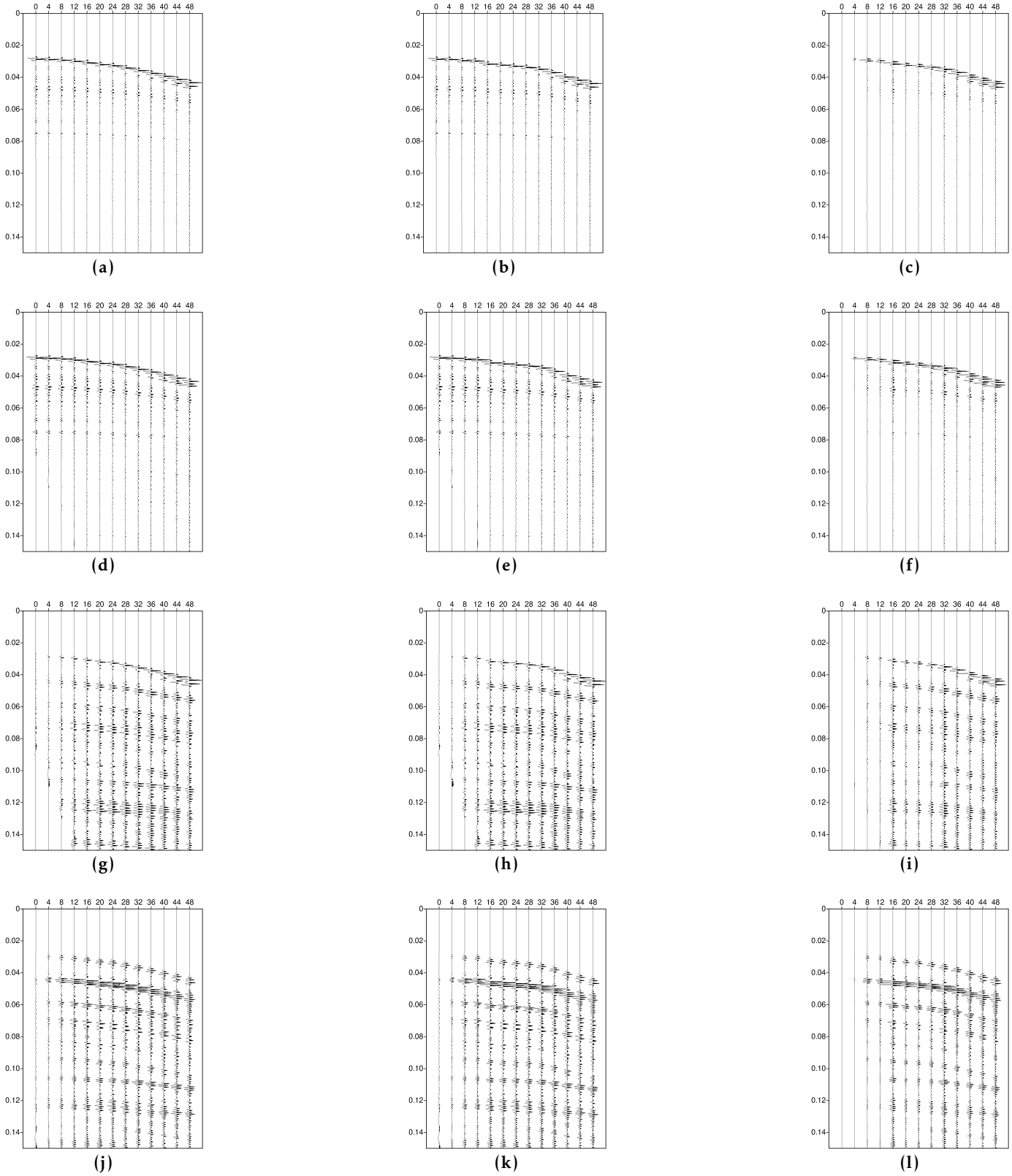


**Figure A9.** Wavefields for scenario 5 with adjusted positions. Legend is the same as for Figure A1.

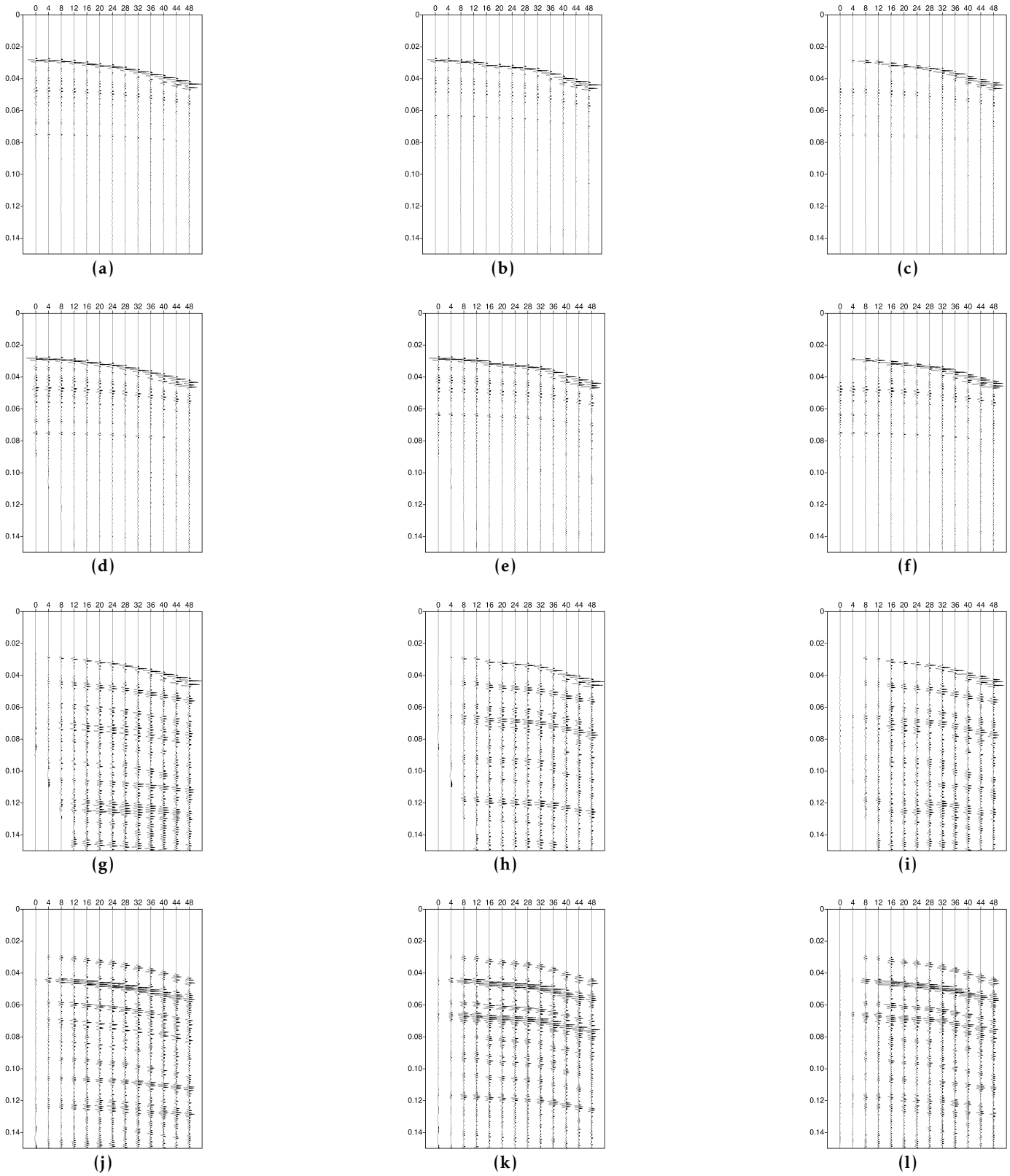


**Figure A10.** Wavefields for scenario 5 with adjusted positions. Legend is the same as for Figure A1.

**References**

Bagriy, I. D., N. V. Maslun, U. Z. Naumenko, D. M. Bozhezha, and S. D. Zubal (2019), Geological-Structural-Thermo-Atmogeochemical Technology for Quick Prediction and Monitoring of Dangerous Geological Processes and Phenomena in the Territory of Ukraine, in *Geology and Mineral Resources of the World Ocean*, pp. 24–47, European Association of Geoscientists & Engineers, https://doi.org/10.3997/2214-4609.201903187.

Berryman, J. G. (1980), Long-wavelength propagation in composite elastic media i. spherical inclusions, *The Journal of the Acoustical Society of America*, *68*(6), 1809–1819, https://doi.org/https://doi.org/10.1121/1.385171.

Bohlen, T. (2002), Parallel 3-D viscoelastic finite difference seismic modelling, *Computers & Geosciences*, *28*(8), 887–899, https://doi.org/https://doi.org/10.1016/S0098-3004(02)00006-7.

Cohen, J. K., and J. W. Stockwell, Jr. (2002), *CWP/SU: Seismic Unix Release 36: a free package for seismic research and processing*, Center for Wave Phenomena, Colorado School of Mines.

Daigle, H., L. L. Worthington, S. P. S. Gulick, and H. J. A. Van Avendonk (2017), Rapid sedimentation and overpressure in shallow sediments of the Bering Trough, offshore southern Alaska, *Journal of Geophysical Research: Solid Earth*, *122*(4), 2457–2477, https://doi.org/https://doi.org/10.1002/2016JB013759.

Dubinya, N., I. Bayuk, A. Hortov, K. Myatchin, A. Pirogova, and P. Shchuplov (2022), Prediction of Overpressure Zones in Marine Sediments Using Rock-Physics and Other Approaches, *Journal of Marine Science and Engineering*, *10*(8), 1127, https://doi.org/https://doi.org/10.3390/jmse10081127.

Dugan, B., and P. B. Flemings (2000), Overpressure and Fluid Flow in the New Jersey Continental Slope: Implications for Slope Failure and Cold Seeps, *Science*, *289*(5477), 288–291, https://doi.org/https://doi.org/10.1126/science.289.5477.288.

Dugan, B., and J. T. Germaine (2008), Near-seafloor overpressure in the deepwater mississippi canyon, northern gulf of mexico, *Geophysical Research Letters*, *35*(2), https://doi.org/https://doi.org/10.1029/2007GL032275.

Dugan, B., and T. C. Sheahan (2012), Offshore sediment overpressures of passive margins: Mechanisms, measurement, and models, *Reviews of Geophysics*, *50*(3), https://doi.org/https://doi.org/10.1029/2011RG000379.

Dvorkin, J., M. Prasad, A. Sakai, and D. Lavoie (1999), Elasticity of marine sediments: Rock physics modeling, *Geophysical Research Letters*, *26*(12), 1781–1784, https://doi.org/https://doi.org/10.1029/1999GL900332.

Fan, C., C. Xu, C. Li, A. Liu, H. Li, J. Hou, X. Zhang, B. Lu, and J. Li (2021), Identification and Prediction of Allo-Source Overpressure Caused by Vertical Transfer: Example from an HTHP Gas Reservoir in the Ledong Slope in the Yinggehai Basin, *Geofluids*, *2021*, 1–20, https://doi.org/https://doi.org/10.1155/2021/6657539.

Finkbeiner, T., M. Zoback, P. Flemings, and B. Stump (2001), Stress, pore pressure, and dynamically constrained hydrocarbon columns in the South Eugene Island 330 field, northern Gulf of Mexico, *AAPG Bulletin*, *85*(6), 1007–1031, https://doi.org/https://doi.org/10.1306/8626CA55-173B-11D7-8645000102C1865D.

Gassmann, F. (1951), Uber die Elastizitat Poroser Medien, *Vierteljahrsschrift der Naturforschenden Gesellschaft in Zürich*, *96*, 1–23.

Grauls, D., and J. Baleix (1994), Role of overpressures and in situ stresses in fault-controlled hydrocarbon migration: a case study, *Marine and Petroleum Geology*, *11*(6), 734–742, https://doi.org/https://doi.org/10.1016/0264-8172(94)90026-4.

Hashin, Z., and S. Shtrikman (1963), A variational approach to the theory of the elastic behaviour of multiphase materials, *Journal of the Mechanics and Physics of Solids*, *11*(2), 127–140, https://doi.org/https://doi.org/10.1016/0022-5096(63)90060-7.

Lee, M. W. (2003), Elastic Properties of Overpressured and Unconsolidated Sediments , *U.S. Geological Survey Bulletin 2214*, pp. 1–10.

Li, C., L. Zhan, and H. Lu (2022a), Mechanisms for Overpressure Development in Marine Sediments, *Journal of Marine Science and Engineering*, *10*(4), 490, https://doi.org/https://doi.org/10.3390/jmse10040490.

Li, C., L. Zhang, X. Luo, B. Wang, Y. Lei, M. Cheng, H. Luo, C. Wang, and L. Yu (2022b), Modeling of Overpressure Generation–Evolution of the Paleogene Source Rock and Implications for the Linnan Sag, Eastern China, *Frontiers in Earth Science*, *10*, https://doi.org/https://doi.org/10.3389/feart.2022.829322.

Liu, H., L. Zhan, and H. Lu (2022), Mechanisms for upward migration of methane in marine sediments, *Frontiers in Marine Science*, *9*, https://doi.org/https://doi.org/10.3389/fmars.2022.1031096.

Mavko, G., T. Mukerji, and J. Dvorkin (2020), *The Rock Physics Handbook*, 3rd ed., 220–308 pp., Cambridge University Press.

Nifuku, K., Y. Kobayashi, Y. Araki, T. Ashida, and T. Taniwaki (2020), Overpressure evolution controlled by spatial and temporal changes in the sedimentation rate: Insights from a basin modelling study in offshore Suriname, *Basin Research*, *33*(2), 1293–1314, https://doi.org/https://doi.org/10.1111/bre.12514.

Pirogova, A. S., S. A. Tikhotskii, M. Y. Tokarev, and A. V. Suchkova (2019), Estimation of Elastic Stress-Related Properties of Bottom Sediments via the Inversion of Very- and Ultra-High-Resolution Seismic Data, *Izvestiya*, *Atmospheric and Oceanic Physics*, *55*(11), 1755–1765, https://doi.org/https://doi.org/10.1134/S0001433819110124.

Saffer, D. M., E. A. Silver, A. T. Fisher, H. Tobin, and K. Moran (2000), Inferred pore pressures at the Costa Rica subduction zone: implications for dewatering processes, *Earth and Planetary Science Letters*, *177*(3–4), 193–207, https://doi.org/https://doi.org/10.1016/S0012-821X(00)00048-0.

Schneider, J., P. B. Flemings, B. Dugan, H. Long, and J. T. Germaine (2009), Overpressure and consolidation near the seafloor of Brazos-Trinity Basin IV, northwest deepwater Gulf of Mexico, *Journal of Geophysical Research: Solid Earth*, *114*(B5), https://doi.org/https://doi.org/10.1029/2008JB005922.

Tikhotskiy, S., I. Bayuk, and N. Dubinya (2023), On the Possibility of Detecting Pore Pressure Changes in Marine Sediments Using Bottom Seismometer Data, *Journal of Marine Science and Engineering*, *11*(9), 1803, https://doi.org/https://doi.org/10.3390/jmse11091803.

Tingay, M. R., R. R. Hillis, R. E. Swarbrick, C. K. Morley, and A. R. Damit (2007), "Vertically transferred" overpressures in Brunei: Evidence for a new mechanism for the formation of high-magnitude overpressure, *Geology*, *35*(11), 1023–1026, https://doi.org/https://doi.org/10.1130/G23906A.1.

Tingay, M. R. P., R. R. Hillis, R. E. Swarbrick, C. K. Morley, and A. R. Damit (2009), Origin of overpressure and pore-pressure prediction in the baram province, brunei, *AAPG Bulletin*, *93*(1), 51–74, https://doi.org/https://doi.org/10.1306/08080808016.

Wangen, M. (2021), Models of overpressure build-up in shallow sediments by glacial deposition and glacial loading with respect to chimney formation, *Modeling Earth Systems and Environment*, *8*(1), 1227–1242, https://doi.org/https://doi.org/10.1007/s40808-020-01064-6.

Yin, X., S. Li, J. Yang, and Q. Zhang (2002), Correlations between Overpressure Fluid Activity and Fault System in Yinggehai Basin, *Acta Geoscientia Sinica*, *23*(2), 141–146, https://doi.org/https://doi.org/10.3321/j.issn:1006-3021.2002.02.008 (in Chinese).

Zhang, Y., M. Person, V. Voller, D. Cohen, J. McIntosh, and R. Grapenthin (2018), Hydromechanical Impacts of Pleistocene Glaciations on Pore Fluid Pressure Evolution, Rock Failure, and Brine Migration Within Sedimentary Basins and the Crystalline Basement, *Water Resources Research*, *54*(10), 7577–7602, https://doi.org/https://doi.org/10.1029/2017WR022464.